#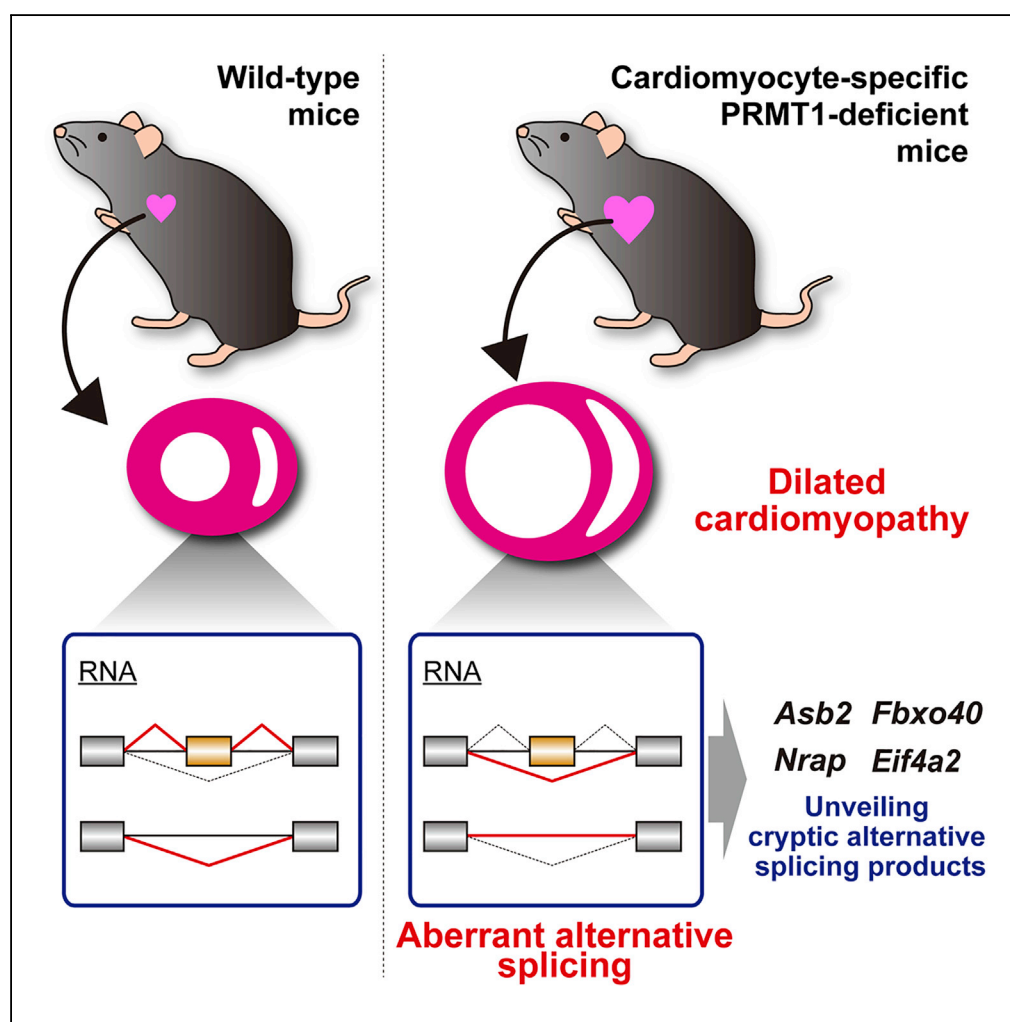 PRMT1 Deficiency in Mouse Juvenile Heart Induces Dilated Cardiomyopathy and Reveals Cryptic Alternative Splicing Products

	Masafumi MURATANI, Weizhe Lu, Misuzu Hashimoto, Natsumi Ono, Kazuya MURATA, Kana Nishikata, Jun-Dal Kim, Shizufumi Ebihara, Junji ISHIDA, Akiyoshi FUKAMIZU

Article

PRMT1 Deficiency in Mouse Juvenile Heart Induces Dilated Cardiomyopathy and Reveals Cryptic Alternative Splicing Products

Kazuya Murata, Weizhe Lu, Misuzu Hashimoto, ..., Shizufumi Ebihara, Junji Ishida, Akiyoshi Fukamizu

akif@tara.tsukuba.ac.jp

HIGHLIGHTS

PRMT1 deficiency in cardiomyocytes causes dilated cardiomyopathy in juvenile mice

PRMT1-deficient heart shows abnormal alternative splicing patterns

Previously undefined cardiac splicing events are revealed by transcriptome analysis

eIF4A2 isoforms are differentially ubiquitinated and degraded

DATA AND SOFTWARE AVAILABILITY

GSE112938

Article

PRMT1 Deficiency in Mouse Juvenile Heart Induces Dilated Cardiomyopathy and Reveals Cryptic Alternative Splicing Products

Kazuya Murata,[1,9] Weizhe Lu,[2] Misuzu Hashimoto,[2,3] Natsumi Ono,[4] Masafumi Muratani,[5,6] Kana Nishikata,[7] Jun-Dal Kim,[1,4] Shizufumi Ebihara,[7] Junji Ishida,[1,4] and Akiyoshi Fukamizu[1,4,8,10,]*

SUMMARY

Protein arginine methyltransferase 1 (PRMT1) catalyzes the asymmetric dimethylation of arginine residues in proteins and methylation of various RNA-binding proteins and is associated with alternative splicing *in vitro*. Although PRMT1 has essential *in vivo* roles in embryonic development, CNS development, and skeletal muscle regeneration, the functional importance of PRMT1 in the heart remains to be elucidated. Here, we report that juvenile cardiomyocyte-specific PRMT1-deficient mice develop severe dilated cardiomyopathy and exhibit aberrant cardiac alternative splicing. Furthermore, we identified previously undefined cardiac alternative splicing isoforms of four genes (*Asb2*, *Fbxo40*, *Nrap*, and *Eif4a2*) in PRMT1-cKO mice and revealed that eIF4A2 protein isoforms translated from alternatively spliced mRNA were differentially ubiquitinated and degraded by the ubiquitin-proteasome system. These findings highlight the essential roles of PRMT1 in cardiac homeostasis and alternative splicing regulation.

INTRODUCTION

Arginine methylation, a post-translational modification, is found in a broad range of proteins, including histones, transcription factors, membrane proteins, and RNA-binding proteins (RBPs) (Yang and Bedford, 2013). In mammalian cells, 10 protein arginine methyltransferases (PRMTs) are responsible for arginine methylation and have been classified into three groups according to their catalytic machinery (Yang and Bedford, 2013; Hatanaka et al., 2017). PRMT1, PRMT2, PRMT3, PRMT4 (also called CARM1), PRMT6, PRMT8, and METTL23 belong to type I PRMTs, which catalyze the formation of mono-methylarginine and asymmetric dimethylarginine. PRMT5 and PRMT9 are known as type II PRMTs, which are capable of producing mono-methylarginine and symmetric dimethylarginine (Hadjikyriacou et al., 2015; Yang et al., 2015). PRMT7 has been characterized as a type III enzyme synthesizing only mono-methylarginine (Zurita-Lopez et al., 2012).

PRMT1, a ubiquitously expressed type I enzyme, was the first identified PRMT, and it regulates a wide variety of cellular processes, such as transcription, DNA damage response, and signal transduction (Wang et al., 2001; Yamagata et al., 2008; Yang and Bedford, 2013). The *in vivo* functions of PRMT1 were not identified in mammals for a long time, because conventional PRMT1-deficient mice showed early embryonic lethality (Pawlak et al., 2000). In recent years, two independent reports using heterozygous *Prmt1*-deficient mice revealed that PRMT1 controls hepatic gluconeogenesis and neuronal excitability in the CNS (Choi et al., 2012; Kim et al., 2016). Another group reported that lack of PRMT1 in murine muscle stem cells impairs muscle regeneration (Blanc et al., 2017). On the other hand, we demonstrated that CNS-specific PRMT1-deficient mice exhibited hypomyelination, indicating a vital role of PRMT1 in oligodendrocyte development (Hashimoto et al., 2016). Furthermore, we also showed that loss of PRMT1 in vascular endothelial cells results in angiodysplasia in mouse embryo (Ishimaru et al., 2017). Thus, an increasing number of studies indicate that PRMT1 has crucial roles in multiple tissue functions and development.

Several reports have investigated the protein expression levels of PRMTs in the rodent heart and show that the cardiac tissue expresses PRMT1, PRMT3, PRMT4, PRMT5, and PRMT7 (Bulau et al., 2007). In addition, PRMT5 directly methylates GATA4 transcription factor, and inhibits phenylephrine-induced cardiomyocyte hypertrophy in neonatal rat ventricular myocytes (Chen et al., 2014). PRMT4 has been shown to regulate aging-related autophagy in mouse heart (Li et al., 2017). Interestingly, cardiac PRMT1 expression is

increased in patients with coronary artery disease and in rats with isoproterenol-induced heart failure (Chen et al., 2006; Li et al., 2012), suggesting the importance of PRMT1 in the heart. However, the physiological function of PRMT1 in the heart remains to be elucidated.

A number of reports have demonstrated that genetic deletion of RBP causes abnormal alternative splicing, resulting in lethal heart failure (Xu et al., 2005; Guo et al., 2012; Ye et al., 2015; Wei et al., 2015). SRSF1, a serine/arginine-rich family of splicing factors, is essential for the splicing switch of the Ca^{2+}/calmodulin-dependent kinase II δ (*Camk2d*) gene, and its deficiency in mouse cardiomyocytes leads to dilated cardio-myopathy (DCM) (Xu et al., 2005). Moreover, mutations in RNA-binding motif protein 20 (RBM20) gene, a regulator of titin (*Ttn*) mRNA splicing, has been shown to cause human DCM (Guo et al., 2012; Wells et al., 2013; Beqqali et al., 2016). Other reports have shown that hnRNP U and RBFOX2 are necessary for alternative splicing of some genes and maintenance of cardiac function in mouse models (Ye et al., 2015; Wei et al., 2015). Interestingly, using a proteomic approach, it has been shown that many types of RBPs, such as SRSFs, RBMs, hnRNPs, and RBFOXs, are methylated in the arginine residues (Guo et al., 2014). Although it has been reported that PRMT1 methylates various RBPs, including hnRNP A2, hnRNP U, and RBM15 (Nichols et al., 2000; Herrmann et al., 2004; Zhang et al., 2015), there is no *in vivo* evidence that PRMT1 regulates alternative splicing.

In this study, we aimed to assess whether the deletion of PRMT1 affects cardiac functions and alternative splicing events in the heart. To this end, we generated cardiomyocyte-specific PRMT1-deficient mice and found that they display features of heart failure, including contractile dysfunction and cardiac chamber dilation. Furthermore, we also found that the deletion of PRMT1 impairs alternative splicing of mRNA in the heart and detected uncharacterized alternative splicing isoforms in some genes. Finally, we demonstrated that protein products translated from alternatively spliced mRNA variants exhibit distinct ubiquitination status in C2C12 myoblast cells. Our results clarify the essential role of PRMT1 in cardiac homeostasis and alternative splicing.

RESULTS

PRMT1 Is Expressed in Both Cardiomyocytes and Non-myocytes

To elucidate the role of PRMT1 in the heart, we first examined the type of cells expressing PRMT1 using *Prmt1*$^{tm1a\ (EUCOMM)\ Wtsi}$ knockin (PRMT1^{KI}) mice (Skarnes et al., 2011). *Prmt1*$^{tm1a\ (EUCOMM)\ Wtsi}$ allele contains FRT-flanked *lacZ*/neomycin sequence within intron 3 in *Prmt1* gene. As PRMT1^{KI} mice express β-galactosi-dase (β-gal) driven by endogenous *Prmt1* promoter, we performed X-gal staining using hearts from em-bryos and adult mice. At embryonic day 19, β-gal activity was ubiquitously detected in the heart section, including atrial and ventricular walls (Figure 1A). In the adult mice, β-gal activity was found in the center of cardiomyocytes and in the vascular wall cells (Figure 1B). To further investigate PRMT1-expressing cell types, we examined the protein expression levels of PRMT1 in isolated primary cardiomyocytes and non-myocytes from cardiac tissues of C57BL/6 mice. Consistent with the results of X-gal staining, PRMT1 was expressed in cardiomyocytes and non-myocytes in the mouse heart (Figure 1C).

Cardiomyocyte-Specific PRMT1 Deletion Causes Dilated Cardiomyopathy in Juvenile Mice

To examine the function of PRMT1 in cardiomyocytes, we generated cardiomyocyte-specific PRMT1-defi-cient (hereafter referred to as PRMT1-cKO) mice. These mice were obtained by crossing *Prmt1*$^{flox/flox}$ mice with α myosin heavy chain (αMHC)-Cre transgenic mice (Figures 1D and 1E). PRMT1 protein levels were decreased in the heart of PRMT1-cKO mice compared with *Prmt1*$^{flox/flox}$ (control) mice (Figure 1F). Immu-nohistochemical analysis revealed that PRMT1 is mainly expressed in the nuclei of cardiomyocytes and non-myocytes in control mice (Figure 1G, upper panels). Furthermore, in both control and cKO mice, non-myocytes showed various levels of green fluorescence, suggesting that PRMT1 expression levels are highly heterogeneous among non-myocytes depending on the cell types (Figure 1G, arrows). We found that the signals of PRMT1 were dramatically reduced in the cardiomyocytes of PRMT1-cKO mice, whereas non-myocytes normally expressed PRMT1 (Figure 1G, lower panels). These data clearly show that PRMT1 is specifically deleted in the cardiomyocytes of PRMT1-cKO mice.

To determine the influence of PRMT1 deletion on the heart, we analyzed the cardiac morphology and func-tion in PRMT1-cKO mice. Although PRMT1-cKO mice were born in a normal Mendelian ratio (data not shown), they died within 60 days of birth (Figure 2A). Heart weight and heart/body weight ratio were significantly increased in 6-week-old PRMT1-cKO mice compared with age-matched control and *Prmt1*
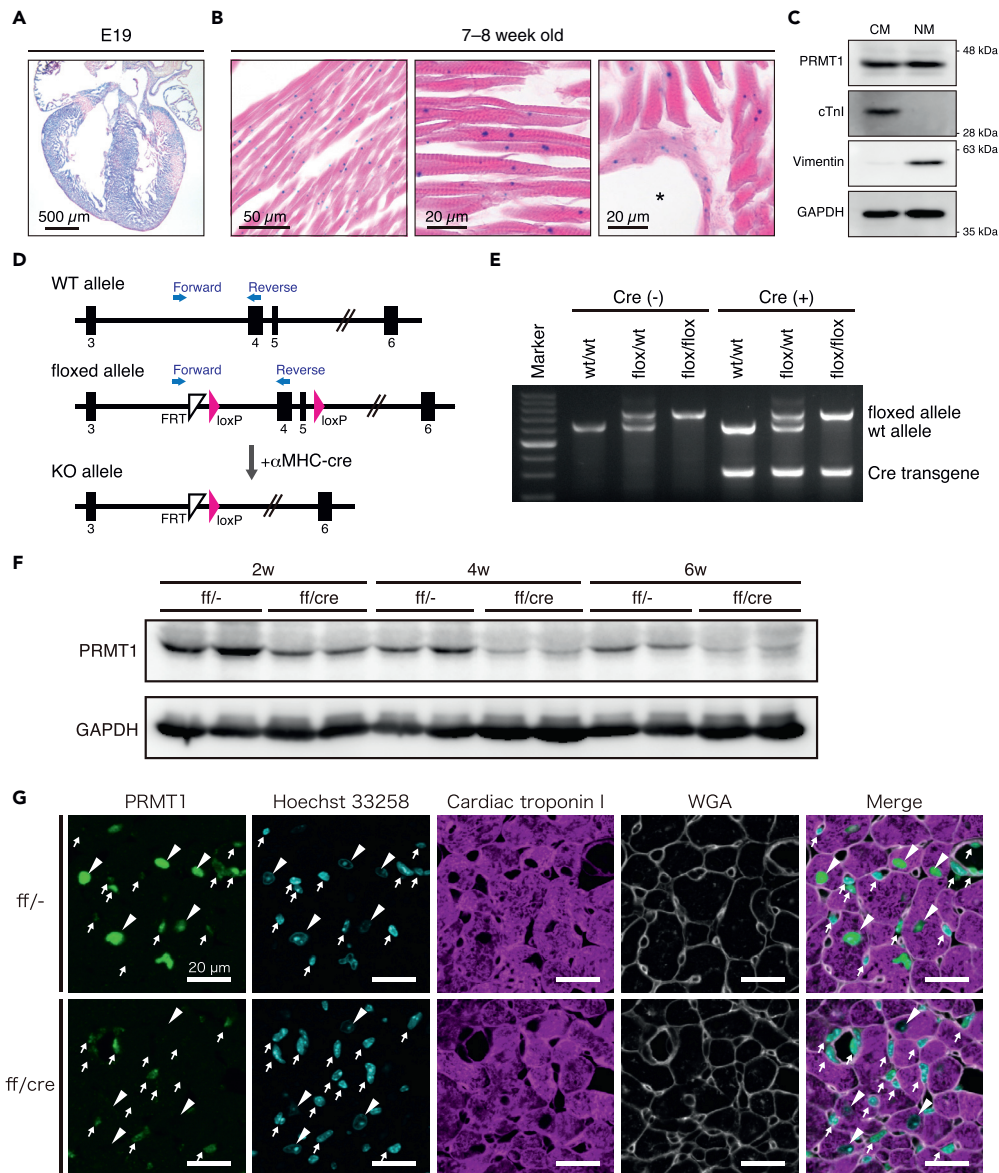
Figure 1. Generation of Cardiomyocyte-Specific PRMT1-Deficient Mice

(A and B) X-gal staining of (A) fetal and (B) adult hearts in PRMT1[KI] mice. The asterisk indicates cardiac artery.

(C) Western blotting of PRMT1 in neonatal mouse cardiomyocytes (CM) and non-myocytes (NM). Cardiac troponin I (cTnI) and vimentin were used as specific markers for CM and NM, respectively. GAPDH was used as loading control.

(D) Schematic diagram of *Prmt1* gene targeting. Black rectangles indicate exons of *Prmt1*, and blue allows show primer set for genotyping.

(E) Representative images of genotyping in PRMT1-cKO mice.

(F) Western blotting analysis of PRMT1 in the hearts of control (ff/-) and PRMT1-cKO (ff/cre) mice. The hearts were harvested from 2-, 4-, and 6-week-old (shown as 2w, 4w, and 6w in the figure) mice.

(G) Representative images of cardiac sections stained with anti-PRMT1 antibody (green), Hoechst 33258 (blue), anti-cardiac troponin I antibody (magenta), and WGA (gray). Arrowheads indicate nuclei of cardiomyocytes. Arrows indicate non-cardiomyocytes.

hetero-deficient mice (Figures 2B and 2C). PRMT1-cKO mice exhibited marked cardiac chamber dilation and fibrosis at 6 weeks of age (Figure 2D, lower panels). Cardiac systolic function of PRMT1-cKO mice began to reduce within 4 weeks after birth, and further reduction was observed in 6-week-old mice (Figure 2E). Furthermore, expression levels of βMHC (*Myh7*), ANP (*Nppa*), and BNP (*Nppb*) genes, which are

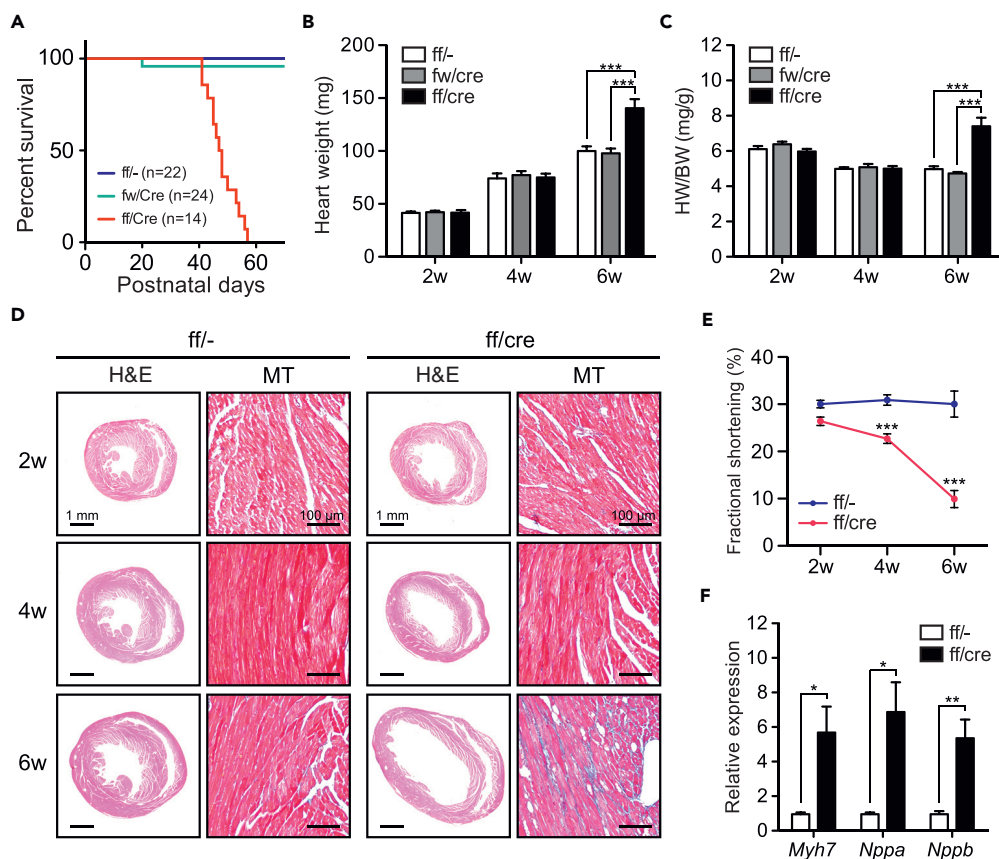**Figure 2. Dilated Cardiomyopathy of PRMT1-cKO Mice**

(A) Survival rate of control, heterozygous (fw/cre), and PRMT1-cKO mice.

(B and C) (B) Heart weight and (C) heart weight/body weight ratio (HW/BW) of 2-, 4-, and 6-week-old mice (n = 4–6).

(D) H&E and Masson's trichrome (MT) staining of the hearts at different ages.

(E) Cardiac contractility of control and PRMT1-cKO mice at different ages.

(F) Gene expression analysis for marker genes of cardiac dysfunction in the heart of 4-week-old control and PRMT1-cKO mice (n = 4).

All data are presented as mean ± SEM. *p < 0.05, **p < 0.01, ***p < 0.001 compared with age-matched control mice.

well-characterized markers of heart failure, were significantly elevated in the heart of PRMT1-cKO mice at 4 weeks of age (Figure 2F).

We further conducted a comprehensive analysis of gene expression changes in the heart of 6-week-old PRMT1-cKO mice using RNA sequencing (RNA-seq). Gene expression analysis identified 2,037 differentially expressed genes between control and PRMT1-cKO mice: 1,044 genes were upregulated and 993 genes were downregulated (Table S1, Figures S1A and S1B). Consistent with the results of histological analysis, fibrosis-related genes, such as *Tgfb2*, *Ctgf*, and collagen family, were induced in the heart of PRMT1-cKO mice (Table S1). On the other hand, Kyoto Encyclopedia of Genes and Genomics pathway analysis of decreased genes showed an enrichment in pathways related to energy metabolism, mitochondrial function, and DCM (Figure S1C). This transcriptional profile of the PRMT1-cKO mice coincides with that of a DCM mouse model carrying a missense mutation in the phospholamban gene (Burke et al., 2016). These observations clearly demonstrated that juvenile PRMT1-cKO mice develop lethal DCM and that PRMT1 plays critical roles in maintaining cardiac homeostasis.

Cardiomyocyte-Specific Loss of PRMT1 Causes Aberrant Alternative Splicing of mRNA in the Heart

To examine the effect of PRMT1 deletion on cardiac alternative splicing, we focused on the known alternative splicing events that are observed in the loss of function or the gain of function in animal models

for RBPs in the heart (Table S2), and analyzed RNA-seq data. Sashimi plots revealed differences in exon usage of several genes between control and PRMT1-cKO mice at 6 weeks of age (Figure 3A). These results were confirmed by RT-PCR using the heart of 4-week-old mice, indicating that alternative splicing abnormality occurs in the early stage of cardiac pathogenesis in PRMT1-cKO mice (Figures 3B and 3C).

Alternative splicing defects or mutations of *Ttn* gene, which encodes a giant sarcomeric protein, are closely associated with DCM (Guo et al., 2012; Herman et al., 2012; Schafer et al., 2017). Consistent with a previous work using rat model (Li et al., 2013), intron retention was observed within the regions encoding middle Ig domains and PEVK regions in the heart of control mice, whereas it was clearly reduced in those of PRMT1-cKO mice aged 6 weeks (Figures 3D and 3E). Similar changes in alternative splicing of *Ttn* gene have been found in RBM20 knockout rats and cardiomyocyte-specific hnRNP U-deficient mice (Guo et al., 2012; Li et al., 2013; Ye et al., 2015). These results indicate that PRMT1 modulates cardiac alternative splicing events, regulated by a wide-range of RBPs.

The Heart of PRMT1-cKO Mouse Provides Valuable Tissues for Exploration of Unidentified Alternative Splicing Events

To further investigate the effects of PRMT1 deletion on alternative splicing in the heart, we searched for the genes that display abnormal splicing pattern in PRMT1-cKO mice. From RNA-seq data, we extracted genes that have differences in expression levels of splicing isoform between control and PRMT1-cKO mice and found 74 candidate genes (Table S3). A gene ontology analysis of the 74 candidates showed enrichment of genes implicated in muscle development, such as muscle cell development, myofibril assembly, and actin cytoskeleton organization (Figure S2). This hallmark was similar to that of some RBP-deficient animals (Guo et al., 2012; Wei et al., 2015; Dixon et al., 2015). Among the 74 genes, the alternative splicing of *Ttn*, *Lmo7*, *Tnnt2*, *Rtn4*, and *Obscn* has been shown to be directly regulated by RBM20 (Maatz et al., 2014). The alterations in *Pdlim5* and *Ldb3* splicing have been observed in RBM20-, RBFOX2-, and MBNL1-deficient animals (Guo et al., 2012; Wei et al., 2015; Dixon et al., 2015). In addition, alternative splicing events of *Pkm*, *Sptan1*, *Ppfibp1*, and *Popdc2* genes in the heart have already been reported (Gao and Cooper, 2013; Cianci et al., 1999; Kalsotra et al., 2008). Thus, these results led us to believe that our screening protocol was sensitive enough to pick up other unknown splicing events that occur in the pathologic hearts. Next, we validated those new alternative splicing events that have not been characterized in mouse hearts to date.

ASB2, a component of ECS-type (ElonginBC-Cullin-SOCS box) E3 ligase complex, has been shown to be essential for the cardiomyocyte maturation in zebrafish model (Fukuda et al., 2017). In the heart of PRMT1-cKO mice, a large number of reads were detected following *Asb2* exon 6 compared with control mice, indicating the existence of the extended form of exon 6 (Figure 4A). This extended exon 6 has not been registered in the NCBI, Ensembl, or UCSC database. To verify the presence of the novel isoform of exon 6, we designed a primer set for the detection of the extended exon 6 and performed RT-PCR analysis. Although the expression level of the known transcript that includes exons 6 and 7 was slightly but significantly decreased in PRMT1-cKO mice, the extended exon 6 expression was increased in PRMT1-cKO hearts (Figures 4B and 4C). Because the extended exon 6 contains a stop codon and a putative poly(A) signal, this exon may serve as a composite terminal exon (Figure S3A; Tian and Manley, 2013). This suggests that this novel transcript encodes truncated ASB2 protein lacking SOCS box, which is required for the formation of E3 ligase complex (Figure S3A; Okumura et al., 2012).

FBXO40 is a component of SCF (Skp, Cullin, and F box) E3 ligase complex, modulating insulin-like growth factor 1 (IGF1) receptor signaling pathway via ubiquitination of IRS1 in skeletal muscle (Shi et al., 2011). A large part of FBXO40 coding sequence is encoded by exon 3 (Ensembl Transcript ID: ENSMUST00000075869.12). Although most of the *Fbxo40* mRNA was contained in exon 3 in the control hearts, exon 3 skipping was significantly increased in the PRMT1-cKO hearts (Figures 4A–4C).

Nrap (nebulin-related anchoring protein) gene encodes a cytoskeletal protein (Bang and Chen, 2015). It has been reported that the expression of NRAP is upregulated in mouse models of DCM (Ehler et al., 2001). Furthermore, several studies investigated the alternative splicing of *Nrap* exon 12 included in skeletal muscle isoform, but not in cardiac isoform (Mohiddin et al., 2003; Berger et al., 2011). In addition to exon 12, the NCBI database suggests that *Nrap* exon 2 is alternatively spliced (NM_001286552.1); however, this splicing
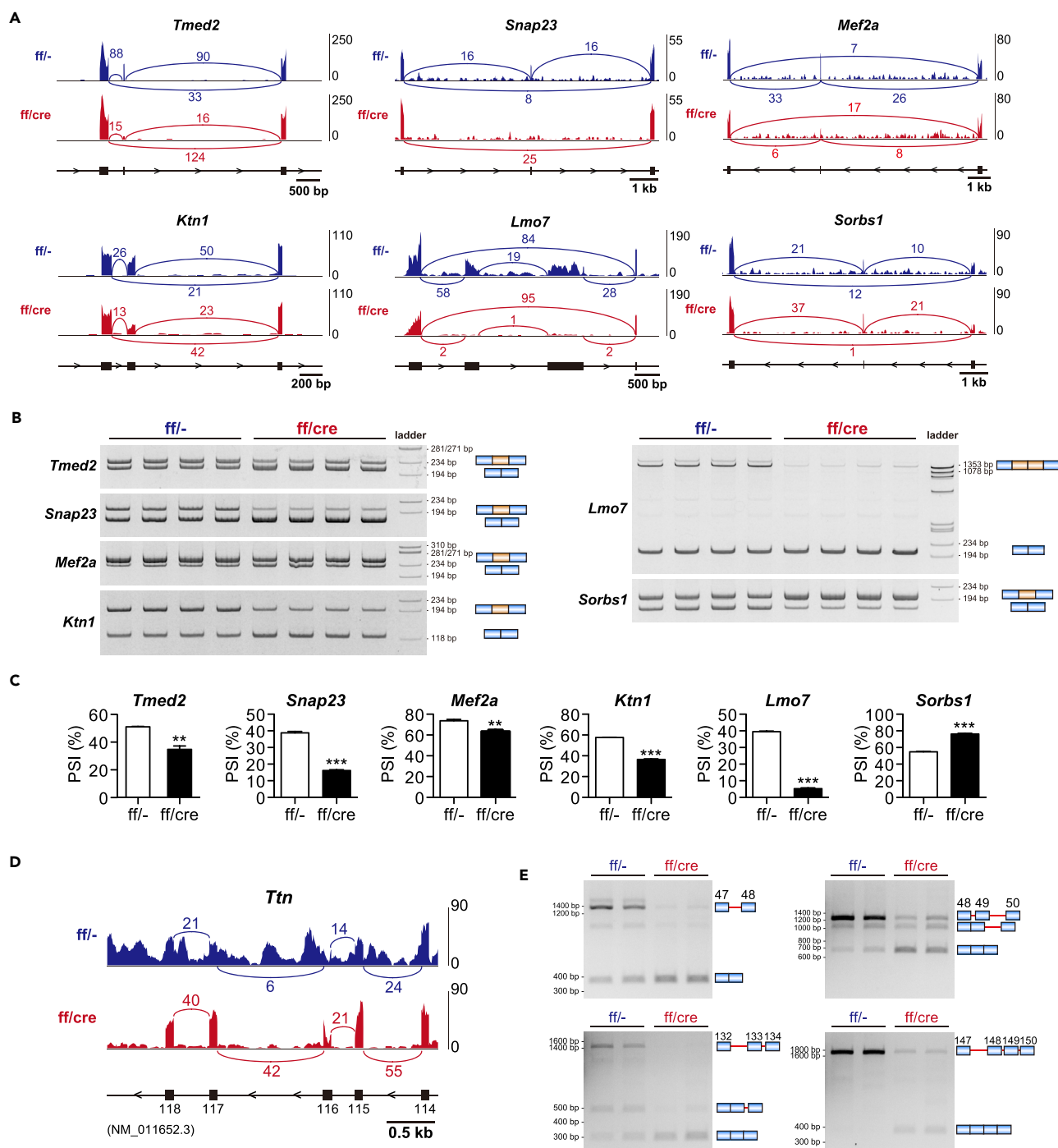
Figure 3. Aberrant Alternative Splicing in the Heart of PRMT1-cKO Mice

(A) Representative images of Sashimi plot depicting alternative splicing pattern in the heart of 6-week-old mice. Read counts for each sample are indicated on the y axis.

(B and C) (B) Gel images of RT-PCR products and (C) percent spliced in (PSI) value calculated from the band intensities for assessing changes in alternative splicing in the heart of 4-week-old mice (n = 4).

(D) Representative images of Sashimi plot depicting alternative splicing of *Titin* (*Ttn*) gene in the heart of 6-week-old mice. Read counts for each sample are indicated on the y axis.

(E) Gel images of RT-PCR products for *Titin* gene. Blue rectangles and red lines indicate exons and introns of *Titin* gene, respectively.

All data are presented as mean ± SEM. **p < 0.01, ***p < 0.001 compared with control mice.
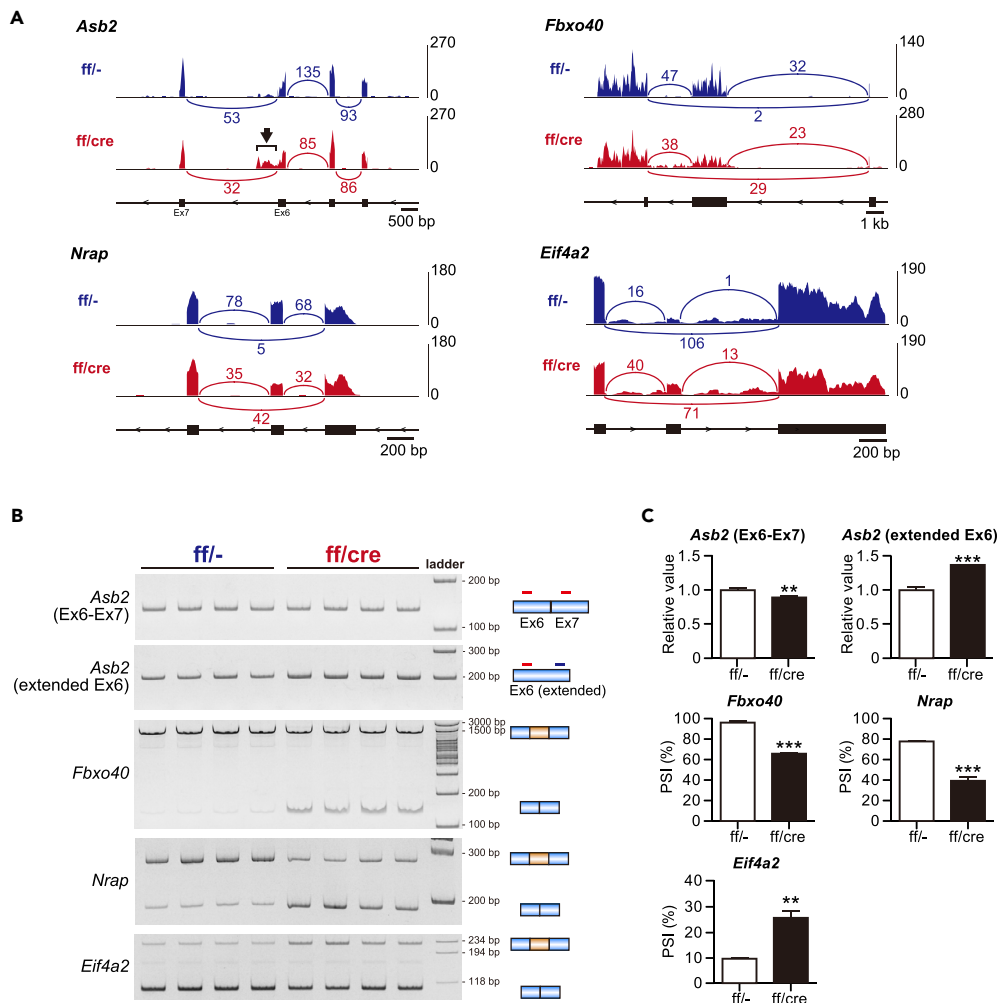
Figure 4. Novel Alternative Splicing Events in the Heart

(A) Representative Sashimi plots depicting alternative splicing pattern in the heart of 6-week-old mice. Read counts for each sample are indicated on the y axis.

(B and C) (B) Gel images of RT-PCR products and (C) relative expression (for *Asb2*) or PSI value (for *Fbxo40*, *Nrap*, and *Eif4a2*) calculated from the band intensities in the heart of 4-week-old mice (n = 4).

All data are presented as mean $\pm$ SEM. **$p < 0.01$, ***$p < 0.001$ compared with control mice.

event has not been characterized in the heart. Although alternative splicing defect of *Nrap* has been found in the heart of *Rbfox2*-KO mice, a model of DCM, which exons are affected by *Rbfox2* deficiency in the heart has not been addressed (Wei et al., 2015). We found that exon skipping of *Nrap* exon 2, encoding an LIM domain of NRAP protein, was significantly increased in PRMT1-cKO mice (Figures 4A–4C).

Eif4a2 gene encodes eIF4A2 DEAD-box RNA helicase associated with translation initiation, microRNA-mediated gene repression, and stress granule formation (Meijer et al., 2013; Jongjitwimol et al., 2016). A previous report demonstrated that knockdown of splicing factor U2AF65 or U2AF35 induces the inclusion of a 107-nucleotide (nt) exon of *EIF4A2* in HeLa cells (Shao et al., 2014). Importantly, the exon-intron structure of eIF4A2 gene is highly conserved between human and mouse (Figure S3B, a–c). In the PRMT1-cKO mice, the 107-nt exon inclusion of *Eif4a2* was significantly increased compared with control mice (Figures 4A–4C).

Taken together, we discovered previously unrecognized cardiac alternative splicing events through the use of PRMT1-cKO mice.

Figure 5. Differential Ubiquitination Status of eIF4A2 Isoforms

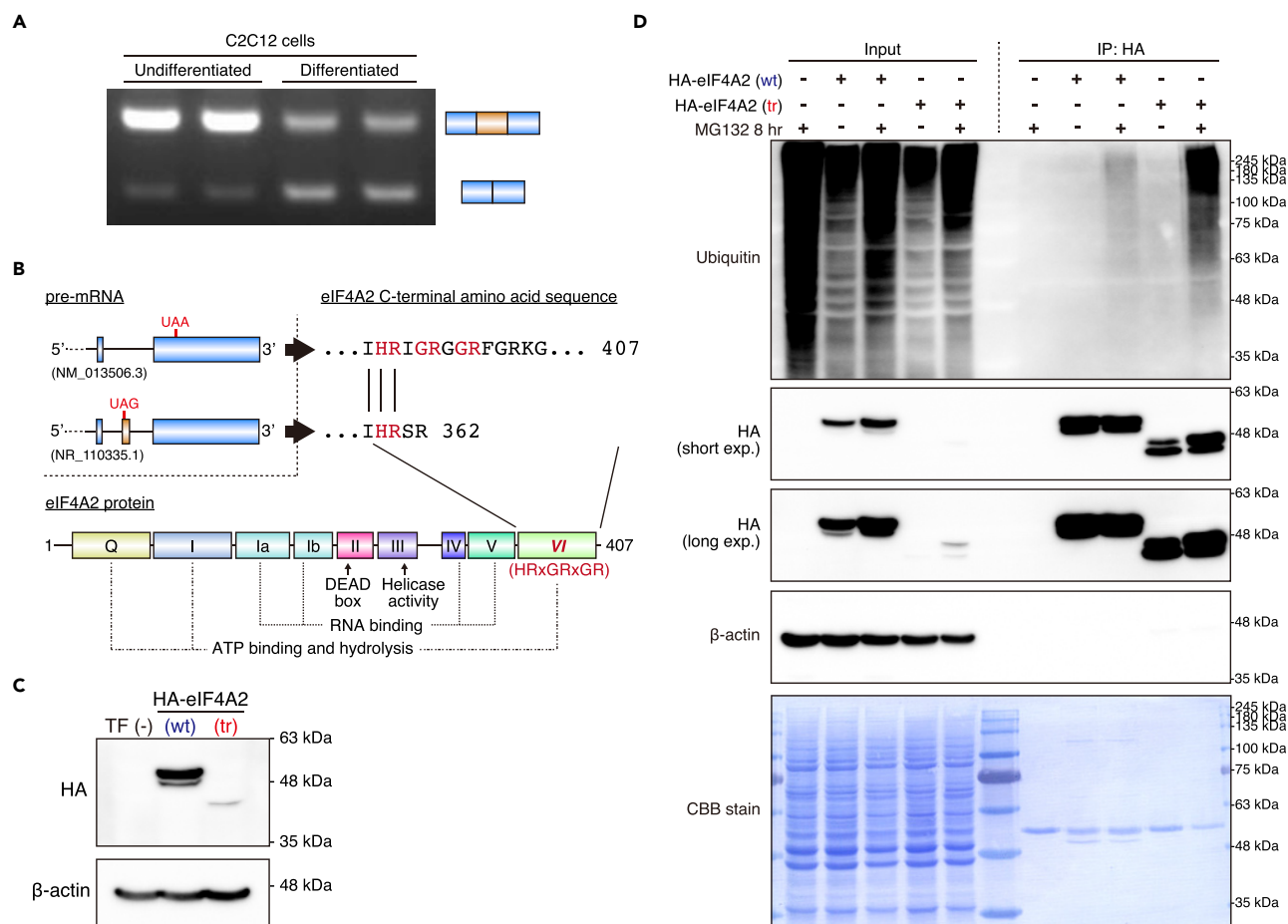(A) RT-PCR analysis for detecting *Eif4a2* alternative splicing in undifferentiated and differentiated C2C12 cells.

(B) Schematic diagrams of *Eif4a2* pre-mRNA 3' end, C-terminal sequences of eIF4A2, and eIF4A2 protein domains.

(C) Western blot analysis of HA-eIF4A2 wild-type (wt) and truncated (tr) isoforms in C2C12 cells 24 hr after transfection. β-Actin was used as a loading control.

(D) Immunoprecipitation assay for detecting ubiquitination of HA-eIF4A2 isoforms in C2C12 cells. At 16 hr after transfection, cells were treated with MG132 (10 μM) for 8 hr.

eIF4A2 Isoforms Are Differentially Ubiquitinated and Degraded in C2C12 Cells

Finally, we explored the significance of alternative splicing of *Eif4a2* under more physiological conditions. It has been reported that *Eif4a2* mRNA expression is increased in differentiating C2C12 mouse myoblast cells, and that double knockdown of *Eif4a1* and *Eif4a2* suppresses myoblast differentiation into myotubes (Galicia-Vazquez et al., 2014). The differentiation process of C2C12 cells is intimately involved in alternative splicing (Bland et al., 2010; Singh et al., 2014), whereas the association between alternative splicing of *Eif4a2* and C2C12 differentiation is undefined. Therefore, we investigated whether C2C12 differentiation is linked to alternative splicing change of *Eif4a2*. We found that the undifferentiated C2C12 cells predominantly expressed long *Eif4a2* transcripts (Figure 5A). Furthermore, the long *Eif4a2* isoform expression was reduced in differentiating C2C12 cells, whereas that of the short *Eif4a2* isoform was markedly increased (Figure 5A). Although changes in alternative splicing of *Eif4a2* were found in PRMT1-deficient hearts (Figure 4) and U2AF knockdown cells (Shao et al., 2014), data suggested that these splicing changes were also induced by physiological stimuli, such as myoblast differentiation.

The NCBI database predicts that the long *Eif4a2* transcript (NR_110335.1), upregulated in the heart of PRMT1-cKO mice (Figure 4), is a candidate for nonsense-mediated mRNA decay (NMD). Indeed, the 107-nt exon of long *Eif4a2* transcript contains a premature termination codon (PTC) positioned more than 50–55 nt upstream of the last exon-exon junction (Figure 5B). However, several reports have

demonstrated that the PTC-containing transcript escapes NMD, and is translated into a truncated protein that plays an important physiological role (Holbrook et al., 2004; Bamber et al., 1999; Donnadieu et al., 2003). Furthermore, our data showed that PTC-containing long *Eif4a2* transcript is expressed at substantial levels in the heart of PRMT1-cKO mice and in undifferentiated C2C12 cells (Figures 4B and 5A), suggesting that long *Eif4a2* transcript is translated into truncated eIF4A2 protein (Figure 5B). Although eIF4A2 possesses motif VI, which probably functions as a trigger of ATP hydrolysis, at its C terminus (Pause and Sonenberg, 1992; Schutz et al., 2008), truncated eIF4A2 isoform partially lacks motif VI (Figure 5B).

To investigate the functional difference of eIF4A2 isoforms, expressed differentially in the heart of control and PRMT1-cKO mice, we generated hemagglutinin (HA)-tagged eIF4A2 (HA-eIF4A2-wt) and HA-tagged truncated-eIF4A2 (HA-eIF4A2-tr) expression vectors. Although equivalent amount of vectors was transfected into C2C12 cells, unexpectedly, the protein level of HA-eIF4A2-tr was remarkably lower than that of HA-eIF4A2-wt (Figure 5C). A previous study showed that eIF4A2 protein is sumoylated on K226 in mammalian cells (Jongjitwimol et al., 2016), whereas some proteomic analyses indicated that eIF4A2 protein contains several ubiquitination sites (Danielsen et al., 2011, Kim et al., 2011; curated information is available on PhosphoSitePlus, a database of post-translational modifications). Therefore, we hypothesized that HA-eIF4A2-tr protein is ubiquitinated and degraded by the ubiquitin-proteasome system. To examine this hypothesis, we treated C2C12 cells with MG132 after transfection and assessed the ubiquitination levels of HA-eIF4A2 isoforms. MG132 treatment increased both HA-eIF4A2-wt and HA-eIF4A2-tr protein levels (Figure 5D, input). Furthermore, poly-ubiquitination of HA-eIF4A2-wt and HA-eIF4A2-tr was detected in MG132-treated C2C12 cells (Figure 5D, immunoprecipitation [IP]: HA). It is noteworthy that HA-eIF4A2-tr protein was highly ubiquitinated compared with HA-eIF4A2-wt (Figure 5D, IP: HA), indicating that the 47 amino acid residues in the C terminus of eIF4A2-wt protect against ubiquitination and subsequent degradation by the ubiquitin-proteasome system.

DISCUSSION

In the present study, we generated cardiomyocyte-specific PRMT1-deficient mice and demonstrated the vital role of PRMT1 in maintaining cardiac function. Moreover, cardiac alternative splicing was disturbed in the heart of PRMT1-cKO mice, indicating the critical role of PRMT1 in the regulation of alternative splicing *in vivo*. In addition, using this animal model, we successfully detected novel alternative splicing products in the heart.

PRMT1 Is Essential for Cardiac Development in Mice

Accumulating evidence demonstrates that PRMT1, a dominant type I PRMT in mammalian cells, controls tissue development, regeneration, and homeostasis *in vivo* (Hashimoto et al., 2016; Blanc et al., 2017). In the present study, we showed that cardiomyocyte-specific deletion of PRMT1 provoked DCM in juvenile mice. Although PRMT1 has been suggested to be involved in the pathogenesis of heart diseases via overproduction of free asymmetric dimethylarginine followed by its nitric oxide synthase (NOS)-inhibiting effect (Haghikia et al., 2011; Li et al., 2012), our data clearly demonstrated that PRMT1 has essential roles in cardiac development and homeostasis under physiological conditions. Despite the parallel expression of PRMT1 in cardiomyocytes and non-myocytes, PRMT1 deficiency in cardiomyocytes led to DCM in juvenile mice, demonstrating an indispensable role of arginine methylation catalyzed by PRMT1 in cardiomyocytes.

Association between PRMT1 and Cardiac Splicing Regulation

In the postnatal heart, many physiological and structural changes occur, becoming fully functional by adulthood. Although these processes are transcriptionally regulated, alternative splicing also participates in postnatal cardiac development (Baralle and Giudice, 2017). Interestingly, it has been demonstrated that the majority of alternative splicing transitions in cardiomyocytes occur during the first 4 weeks after birth in mice (Giudice et al., 2014). In the present study, we found that PRMT1-cKO mice showed cardiac alternative splicing defects and reduction of cardiac contractility at 4 weeks after birth. We therefore postulated that alternative splicing transition fails in PRMT1-cKO mice. Indeed, we showed that exon skipping of *Tmed2* and *Snap23* was significantly increased in 4-week-old PRMT1-cKO mice (Figures 3B and 3C); these splicing patterns resemble the feature in neonatal hearts (Giudice et al., 2014). These observations suggest that PRMT1 regulates alternative splicing transition in the postnatal hearts.

In this study, we found and validated the four novel splicing events in the heart (Figure 4). Among these, we discovered a new *Asb2* isoform that is not registered in the NCBI, Ensemble, or UCSC database. This novel

Asb2 transcript, which has the extended exon 6 containing a stop codon and a putative poly(A) signal, seems to encode truncated ASB2 protein that lacks SOCS box, suggesting the failure to form E3 ligase complex. On the other hand, ankyrin repeat, a putative substrate recognition motif (Li et al., 2006; Andresen et al., 2014), partially remained in truncated ASB2 protein. Therefore, this truncated ASB2 might function as a dominant-negative isoform to trap substrates. To detect the truncated ASB2 protein, we used commercially available anti-ASB2 antibody that is raised against the N-terminal of ASB2. We were unable to confirm the expression of truncated ASB2 protein in cardiac lysate, whereas weak signal from the full-length ASB2 protein was seen (data not shown), probably because of a lower expression level of truncated ASB2 than full-length protein. Since the expression level of novel *Asb2* isoform was increased in the PRMT1-deficient hearts, PRMT1 may be involved in determining alternative polyadenylation sites in the cardiomyocytes.

Although splicing events of three other genes (*Fbxo40*, *Nrap*, and *Eif4a2*) are recorded in at least one database, there is no evidence demonstrating that these splicing events actually occur in the hearts. It has been reported that FBXO40, a component of SCF E3 ligase complex, regulates IGF1 signaling in the skeletal muscle (Shi et al., 2011). FBXO40 is also expressed in human and rodent hearts (Ye et al., 2007), but its function remains unclear. We found that skipping of the exon encoding a large part of FBXO40 protein was significantly increased in the PRMT1-cKO heart (Figures 4B and 4C). The Ensembl database predicts that this transcript does not contain an open reading frame, suggesting that this short form of *Fbxo40* transcript exists as long non-coding RNA (lncRNA). Interestingly, a recent study revealed that lncRNA, which is produced by alternative splicing of protein-coding gene, plays an important role in tumor progression (Grelet et al., 2017). This raises the possibility that lnc-*Fbxo40* has pathophysiological roles in the heart, and PRMT1 acts as a molecular switch to regulate *Fbxo40* gene function. However, further studies are needed to confirm whether the short form of *Fbxo40* transcript functions as an lncRNA.

We showed that the usage of *Nrap* exon 2 was significantly decreased in the heart of PRMT1-cKO mice (Figures 4B and 4C). *Nrap* transcript that lacks exon 2 encodes an NRAP protein deficient for the LIM domain. NRAP is dominantly expressed in cardiac and skeletal muscles, and is upregulated in the heart of DCM mouse models (Bang and Chen, 2015). NRAP is localized in Z-disk precursors during myofibrillogenesis, whereas specific localization of NRAP at the intercalated disks is found in the adult heart (Bang and Chen, 2015). A previous report revealed that the LIM domain of NRAP strongly binds to talin: talin binds the cytoplasmic domain of β1D integrin subunit, whereas NRAP super-repeats bind to actin, suggesting that NRAP is a component of the protein complex that anchors actin filaments to the plasma membrane (Luo et al., 1999). Although integrin and talin are mainly localized in the costamere, they are also found at the intercalated disks in the heart (Israeli-Rosenberg et al., 2014; Manso et al., 2013). Interestingly, a recent study demonstrated that talin1/talin2 double knockout mice exhibit DCM (Manso et al., 2017). These observations suggest that increase in NRAP lacking the LIM domain may affect the mechanotransduction system through the absence of binding to integrin and talin in the intercalated disks and may contribute to cardiac pathogenesis. Because the role of integrin system in the intercalated disks is largely unknown, it is interesting to investigate the implication in *Nrap* isoform shift and the function of NRAP lacking LIM domain in the heart.

It has been shown that knockdown of splicing factor U2AF increases the 107-nt exon inclusion of *EIF4A2* in HeLa cells (Shao et al., 2014). In the present study, we found that this 107-nt exon of mouse *Eif4a2* is alternatively spliced in the heart and C2C12 cells, suggesting that alternative splicing of *Eif4a2* occurs under physiological conditions in the cardiac and skeletal muscle cells. We assumed that long *Eif4a2* transcript encodes truncated eIF4A2 protein and examined its protein function. Unexpectedly, we found that the eIF4A2 protein is constantly ubiquitinated, and that the truncated isoform is more efficiently ubiquitinated and degraded than the eIF4A2-wt protein, indicating that the splicing switch of *Eif4a2* may regulate its protein levels utilizing the ubiquitin-proteasome system. It has been reported that eIF4A is overexpressed in lung and cervical cancer, and inhibitors of eIF4A have antitumor activity (Bhat et al., 2015). Therefore, an understanding of the molecular basis for alternative splicing and ubiquitination of eIF4A2 may provide new insight into the pathogenesis of heart failure, muscle differentiation, and cancer therapy.

PRMT1 Is a Possible Upstream Regulator of RBPs

In the past decade, a number of studies have revealed the critical roles of the RBPs in the cardiac alternative splicing regulation by analyzing genetically engineered mice. On the other hand, we showed that deletion

of PRMT1 impairs the cardiac alternative splicing of a broad spectrum of genes, including already reported genes that are affected by the deletion or mutation of RBPs. These observations raise the possibility that PRMT1 participates in alternative splicing regulation through the methylation of RBPs in the cardiomyocytes. It has been reported that cardiomyocyte-specific deletion of hnRNP U (also known as SAF-A) results in splicing defects and severe DCM (Ye et al., 2015). Importantly, a previous report demonstrated that PRMT1 methylates hnRNP U, whereas arginine methylation of hnRNP U did not affect its nuclear localization (Herrmann et al., 2004). SRSF1 (as known as SF2/ASF) deficiency in cardiomyocytes also contributes to aberrant splicing and DCM (Xu et al., 2005). Although which PRMTs are involved is unknown, arginine methylation controls SRSF1 nuclear localization (Sinha et al., 2010). Furthermore, proteomic analyses suggested that other RBPs that are related to the cardiac alternative splicing, such as RBFOX1, RBFOX2, MBNL1, and SRSF10, have putative arginine methylation sites (Guo et al., 2014; Larsen et al., 2016; Geoghegan et al., 2015). Our results suggest that PRMT1 may serve as a key regulator of RBPs functions, such as nuclear localization, RNA-binding properties, and binding of other splicing factors, in the cardiomyocytes.

Taken together, our findings identify an essential role of PRMT1 in the cardiac alternative splicing *in vivo*, and the heart of PRMT1-cKO mouse is an effective tool for understanding the relationship between alternative splicing regulation and heart failure.

Limitations of the Study

In the present study, we showed that PRMT1 deficiency in cardiomyocytes causes aberrant alternative splicing in the heart. As it is currently not known whether the changes in alternative splicing are due to direct effects of PRMT1 deficiency or secondary consequences (e.g., an influence of DCM), we examined the effect of PRMT1 knockdown on alternative splicing of *Eif4a2* in C2C12 cells. However, we were unable to accurately assess the contribution of PRMT1 to *Eif4a2* splicing in undifferentiated or differentiated C2C12 cells (data not shown). This may be because knockdown of PRMT1 was inefficient for changing *Eif4a2* alternative splicing, or PRMT1 regulates alternative splicing in a cell-type-dependent manner. Therefore, other experimental models are needed to investigate whether the changes in alternative splicing are due to the lack of PRMT1.

METHODS

All methods can be found in the accompanying Transparent Methods supplemental file.

DATA AND SOFTWARE AVAILABILITY

The accession number for the data reported in this study is GEO: GSE112938.

SUPPLEMENTAL INFORMATION

Supplemental Information includes Transparent Methods, three figures, and three tables and can be found with this article online at https://doi.org/10.1016/j.isci.2018.09.023.

AUTHOR CONTRIBUTIONS

Conceptualization, K.M. and A.F.; Methodology, K.M., J.I., and A.F.; Investigation, K.M., W.L., M.H., N.O., and K.N.; Formal Analysis, K.M., M.M., and J.-D.K.; Writing – Original Draft, K.M.; Writing – Review & Editing, K.M., M.H., J.I., and A.F.; Supervision, S.E. and A.F.; Funding Acquisition, A.F.

DECLARATION OF INTERESTS

The authors declare no competing interests.

iScience

CellPress

REFERENCES

Andresen, C.A., Smedegaard, S., Sylvestersen, K.B., Svensson, C., Iglesias-Gato, D., Cazzamali, G., Nielsen, T.K., Nielsen, M.L., and Flores-Morales, A. (2014). Protein interaction screening for the ankyrin repeats and suppressor of cytokine signaling (SOCS) box (ASB) family identify Asb11 as a novel endoplasmic reticulum resident ubiquitin ligase. J. Biol. Chem. *289*, 2043–2054.

Bamber, B.A., Beg, A.A., Twyman, R.E., and Jorgensen, E.M. (1999). The *Caenorhabditis elegans* unc-49 locus encodes multiple subunits of a heteromultimeric GABA receptor. J. Neurosci. *19*, 5348–5359.

Bang, M.L., and Chen, J. (2015). Roles of nebulin family members in the heart. Circ. J. *79*, 2081–2087.

Baralle, F.E., and Giudice, J. (2017). Alternative splicing as a regulator of development and tissue identity. Nat. Rev. Mol. Cell Biol. *18*, 437–451.

Beqqali, A., Bollen, I.A., Rasmussen, T.B., van den Hoogenhof, M.M., van Deutekom, H.W., Schafer, S., Haas, J., Meder, B., Sorensen, K.E., van Oort, R.J., et al. (2016). A mutation in the glutamate-rich region of RNA-binding motif protein 20 causes dilated cardiomyopathy through missplicing of titin and impaired Frank-Starling mechanism. Cardiovasc. Res. *112*, 452–463.

Berger, D.S., Moyer, M., Kliment, G.M., van Lunteren, E., and Ladd, A.N. (2011). Expression of a dominant negative CELF protein in vivo leads to altered muscle organization, fiber size, and subtype. PLoS One *6*, e19274.

Bhat, M., Robichaud, N., Hulea, L., Sonenberg, N., Pelletier, J., and Topisirovic, I. (2015). Targeting the translation machinery in cancer. Nat. Rev. Drug Discov. *14*, 261–278.

Blanc, R.S., Vogel, G., Li, X., Yu, Z., Li, S., and Richard, S. (2017). Arginine methylation by PRMT1 regulates muscle stem cell fate. Mol. Cell. Biol. *37*, https://doi.org/10.1128/MCB.00457-16.

Bland, C.S., Wang, E.T., Vu, A., David, M.P., Castle, J.C., Johnson, J.M., Burge, C.B., and Cooper, T.A. (2010). Global regulation of alternative splicing during myogenic differentiation. Nucleic Acids Res. *38*, 7651–7664.

Bulau, P., Zakrzewicz, D., Kitowska, K., Leiper, J., Gunther, A., Grimminger, F., and Eickelberg, O. (2007). Analysis of methylarginine metabolism in the cardiovascular system identifies the lung as a major source of ADMA. Am. J. Physiol. Lung Cell. Mol. Physiol. *292*, L18–L24.

Burke, M.A., Chang, S., Wakimoto, H., Gorham, J.M., Conner, D.A., Christodoulou, D.C., Parfenov, M.G., DePalma, S.R., Eminaga, S., Konno, T., et al. (2016). Molecular profiling of dilated cardiomyopathy that progresses to heart failure. JCI Insight *1*, e86898.

Chen, M., Yi, B., and Sun, J. (2014). Inhibition of cardiomyocyte hypertrophy by protein arginine methyltransferase 5. J. Biol. Chem. *289*, 24325–24335.

Chen, X., Niroomand, F., Liu, Z., Zankl, A., Katus, H.A., Jahn, L., and Tiefenbacher, C.P. (2006). Expression of nitric oxide related enzymes in coronary heart disease. Basic Res. Cardiol. *101*, 346–353.

Choi, D., Oh, K.J., Han, H.S., Yoon, Y.S., Jung, C.Y., Kim, S.T., and Koo, S.H. (2012). Protein arginine methyltransferase 1 regulates hepatic glucose production in a FoxO1-dependent manner. Hepatology *56*, 1546–1556.

Cianci, C.D., Zhang, Z., Pradhan, D., and Morrow, J.S. (1999). Brain and muscle express a unique alternative transcript of alphaII spectrin. Biochemistry *38*, 15721–15730.

Danielsen, J.M., Sylvestersen, K.B., Bekker-Jensen, S., Szklarczyk, D., Poulsen, J.W., Horn, H., Jensen, L.J., Mailand, N., and Nielsen, M.L. (2011). Mass spectrometric analysis of lysine ubiquitylation reveals promiscuity at site level. Mol. Cell. Proteomics *10*, M110.003590.

Dixon, D.M., Choi, J., El-Ghazali, A., Park, S.Y., Roos, K.P., Jordan, M.C., Fishbein, M.C., Comai, L., and Reddy, S. (2015). Loss of muscleblind-like 1 results in cardiac pathology and persistence of embryonic splice isoforms. Sci. Rep. *5*, 9042.

Donnadieu, E., Jouvin, M.H., Rana, S., Moffatt, M.F., Mockford, E.H., Cookson, W.O., and Kinet, J.P. (2003). Competing functions encoded in the allergy-associated F(c)epsilonRIbeta gene. Immunity *18*, 665–674.

Ehler, E., Horowits, R., Zuppinger, C., Price, R.L., Perriard, E., Leu, M., Caroni, P., Sussman, M., Eppenberger, H.M., and Perriard, J.C. (2001). Alterations at the intercalated disk associated with the absence of muscle LIM protein. Exp. Cell Res. *153*, 763–772.

Fukuda, R., Gunawan, F., Beisaw, A., Jimenez-Amilburu, V., Maischein, H.M., Kostin, S., Kawakami, K., and Stainier, D.Y. (2017). Proteolysis regulates cardiomyocyte maturation and tissue integration. Nat. Commun. *8*, 14495.

Galicia-Vazquez, G., Di Marco, S., Lian, X.J., Ma, J.F., Gallouzi, I.E., and Pelletier, J. (2014). Regulation of eukaryotic initiation factor 4AII by MyoD during murine myogenic cell differentiation. PLoS One *9*, e87237.

Gao, Z., and Cooper, T.A. (2013). Reexpression of pyruvate kinase M2 in type 1 myofibers correlates with altered glucose metabolism in myotonic dystrophy. Proc. Natl. Acad. Sci. U S A *110*, 13570–13575.

Geoghegan, V., Guo, A., Trudgian, D., Thomas, B., and Acuto, O. (2015). Comprehensive identification of arginine methylation in primary T cells reveals regulatory roles in cell signalling. Nat. Commun. *6*, 6758.

Giudice, J., Xia, Z., Wang, E.T., Scavuzzo, M.A., Ward, A.J., Kalsotra, A., Wang, W., Wehrens, X.H., Burge, C.B., Li, W., et al. (2014). Alternative splicing regulates vesicular trafficking genes in cardiomyocytes during postnatal heart development. Nat. Commun. *5*, 3603.

Grelet, S., Link, L.A., Howley, B., Obellianne, C., Palanisamy, V., Gangaraju, V.K., Diehl, J.A., and Howe, P.H. (2017). A regulated PNUTS mRNA to lncRNA splice switch mediates EMT and tumour progression. Nat. Cell Biol. *19*, 1105–1115.

Guo, A., Gu, H., Zhou, J., Mulhern, D., Wang, Y., Lee, K.A., Yang, V., Aguiar, M., Kornhauser, J., Jia, X., et al. (2014). Immunoaffinity enrichment and mass spectrometry analysis of protein methylation. Mol. Cell. Proteomics *13*, 372–387.

Guo, W., Schafer, S., Greaser, M.L., Radke, M.H., Liss, M., Govindarajan, T., Maatz, H., Schulz, H., Li, S., Parrish, A.M., et al. (2012). RBM20, a gene for hereditary cardiomyopathy, regulates titin splicing. Nat. Med. *18*, 766–773.

Hadjikyriacou, A., Yang, Y., Espejo, A., Bedford, M.T., and Clarke, S.G. (2015). Unique features of human protein arginine Methyltransferase 9 (PRMT9) and its substrate RNA splicing factor SF3B2. J. Biol. Chem. *290*, 16723–16743.

Haghikia, A., Missol-Kolka, E., Tsikas, D., Venturini, L., Brundiers, S., Castoldi, M., Muckenthaler, M.U., Eder, M., Stapel, B., Thum, T., et al. (2011). Signal transducer and activator of transcription 3-mediated regulation of miR-199a-5p links cardiomyocyte and endothelial cell function in the heart: a key role for ubiquitin-conjugating enzymes. Eur. Heart J. *32*, 1287–1297.

Hashimoto, M., Murata, K., Ishida, J., Kanou, A., Kasuya, Y., and Fukamizu, A. (2016). Severe hypomyelination and developmental defects are caused in mice lacking protein arginine Methyltransferase 1 (PRMT1) in the central nervous system. J. Biol. Chem. *291*, 2237–2245.

Hatanaka, Y., Tsusaka, T., Shimizu, N., Morita, K., Suzuki, T., Machida, S., Satoh, M., Honda, A., Hirose, M., Kamimura, S., et al. (2017). Histone H3 methylated at arginine 17 is essential for reprogramming the paternal genome in zygotes. Cell Rep. *20*, 2756–2765.

Herman, D.S., Lam, L., Taylor, M.R., Wang, L., Teekakirikul, P., Christodoulou, D., Conner, L., DePalma, S.R., McDonough, B., Sparks, E., et al. (2012). Truncations of titin causing dilated cardiomyopathy. N. Engl. J. Med. *366*, 619–628.

Herrmann, F., Bossert, M., Schwander, A., Akgun, E., and Fackelmayer, F.O. (2004). Arginine methylation of scaffold attachment factor A by heterogeneous nuclear ribonucleoprotein particle-associated PRMT1. J. Biol. Chem. *279*, 48774–48779.

Holbrook, J.A., Neu-Yilik, G., Hentze, M.W., and Kulozik, A.E. (2004). Nonsense-mediated decay approaches the clinic. Nat. Genet. *36*, 801–808.

Ishimaru, T., Ishida, J., Kim, J.D., Mizukami, H., Hara, K., Hashimoto, M., Yagami, K.I., Sugiyama, F., and Fukamizu, A. (2017). Angiodysplasia in embryo lacking protein arginine methyltransferase 1 in vascular endothelial cells. J. Biochem. *161*, 255–258.

Israeli-Rosenberg, S., Manso, A.M., Okada, H., and Ross, R.S. (2014). Integrins and integrin-associated proteins in the cardiac myocyte. Circ. Res. *114*, 572–586.

Jongjitwimol, J., Baldock, R.A., Morley, S.J., and Watts, F.Z. (2016). Sumoylation of eIF4A2 affects stress granule formation. J. Cell Sci. *129*, 2407–2415.

Kalsotra, A., Xiao, X., Ward, A.J., Castle, J.C., Johnson, J.M., Burge, C.B., and Cooper, T.A. (2008). A postnatal switch of CELF and MBNL proteins reprograms alternative splicing in the developing heart. Proc. Natl. Acad. Sci. U S A *105*, 20333–20338.

Kim, H.J., Jeong, M.H., Kim, K.R., Jung, C.Y., Lee, S.Y., Kim, H., Koh, J., Vuong, T.A., Jung, S., Yang, H., et al. (2016). Protein arginine methylation facilitates KCNQ channel-PIP2 interaction leading to seizure suppression. Elife *5*, e17159.

Kim, W., Bennett, E.J., Huttlin, E.L., Guo, A., Li, J., Possemato, A., Sowa, M.E., Rad, R., Rush, J., Comb, M.J., et al. (2011). Systematic and quantitative assessment of the ubiquitin-modified proteome. Mol. Cell *44*, 325–340.

Larsen, S.C., Sylvestersen, K.B., Mund, A., Lyon, D., Mullari, M., Madsen, M.V., Daniel, J.A., Jensen, L.J., and Nielsen, M.L. (2016). Proteome-wide analysis of arginine monomethylation reveals widespread occurrence in human cells. Sci. Signal. *9*, rs9.

Li, C., Yu, L., Xue, H., Yang, Z., Yin, Y., Zhang, B., Chen, M., and Ma, H. (2017). Nuclear AMPK regulated CARM1 stabilization impacts autophagy in aged heart. Biochem. Biophys. Res. Commun. *486*, 398–405.

Li, J., Mahajan, A., and Tsai, M.D. (2006). Ankyrin repeat: a unique motif mediating protein-protein interactions. Biochemistry *45*, 15168–15178.

Li, S., Guo, W., Dewey, C.N., and Greaser, M.L. (2013). Rbm20 regulates titin alternative splicing as a splicing repressor. Nucleic Acids Res. *41*, 2659–2672.

Li, X., Wang, X., Guo, Y., Deng, N., Zheng, P., Xu, Q., Wu, Y., and Dai, G. (2012). Regulation of endothelial nitric oxide synthase and asymmetric dimethylarginine by matrine attenuates isoproterenol-induced acute myocardial injury in rats. J. Pharm. Pharmacol. *64*, 1107–1118.

Luo, G., Herrera, A.H., and Horowits, R. (1999). Molecular interactions of N-RAP, a nebulin-related protein of striated muscle myotendon

junctions and intercalated disks. Biochemistry *38*, 6135–6143.

Maatz, H., Jens, M., Liss, M., Schafer, S., Heinig, M., Kirchner, M., Adami, E., Rintisch, C., Dauksaite, V., Radke, M.H., et al. (2014). RNA-binding protein RBM20 represses splicing to orchestrate cardiac pre-mRNA processing. J. Clin. Invest. *124*, 3419–3430.

Manso, A.M., Li, R., Monkley, S.J., Cruz, N.M., Ong, S., Lao, D.H., Koshman, Y.E., Gu, Y., Peterson, K.L., Chen, J., et al. (2013). Talin1 has unique expression versus talin 2 in the heart and modifies the hypertrophic response to pressure overload. J. Biol. Chem. *288*, 4252–4264.

Manso, A.M., Okada, H., Sakamoto, F.M., Moreno, E., Monkley, S.J., Li, R., Critchley, D.R., and Ross, R.S. (2017). Loss of mouse cardiomyocyte talin-1 and talin-2 leads to beta-1 integrin reduction, costameric instability, and dilated cardiomyopathy. Proc. Natl. Acad. Sci. U S A *114*, E6250–E6259.

Meijer, H.A., Kong, Y.W., Lu, W.T., Wilczynska, A., Spriggs, R.V., Robinson, S.W., Godfrey, J.D., Willis, A.E., and Bushell, M. (2013). Translational repression and eIF4A2 activity are critical for microRNA-mediated gene regulation. Science *340*, 82–85.

Mohiddin, S.A., Lu, S., Cardoso, J.P., Carroll, S., Jha, S., Horowits, R., and Fananapazir, L. (2003). Genomic organization, alternative splicing, and expression of human and mouse N-RAP, a nebulin-related LIM protein of striated muscle. Cell Motil. Cytoskeleton *55*, 200–212.

Nichols, R.C., Wang, X.W., Tang, J., Hamilton, B.J., High, F.A., Herschman, H.R., and Rigby, W.F. (2000). The RGG domain in hnRNP A2 affects subcellular localization. Exp. Cell Res. *256*, 522–532.

Okumura, F., Matsuzaki, M., Nakatsukasa, K., and Kamura, T. (2012). The role of elongin BC-containing ubiquitin ligases. Front. Oncol. *2*, 10.

Pause, A., and Sonenberg, N. (1992). Mutational analysis of a DEAD box RNA helicase: the mammalian translation initiation factor eIF-4A. EMBO J. *11*, 2643–2654.

Pawlak, M.R., Scherer, C.A., Chen, J., Roshon, M.J., and Ruley, H.E. (2000). Arginine N-Methyltransferase 1 is required for early postimplantation mouse development, but cells deficient in the enzyme are viable. Mol. Cell. Biol. *20*, 4859–4869.

Schafer, S., de Marvao, A., Adami, E., Fiedler, L.R., Ng, B., Khin, E., Rackham, O.J., van Heesch, S., Pua, C.J., Kui, M., et al. (2017). Titin-truncating variants affect heart function in disease cohorts and the general population. Nat. Genet. *49*, 46–53.

Schutz, P., Bumann, M., Oberholzer, A.E., Bieniossek, C., Trachsel, H., Altmann, M., and Baumann, U. (2008). Crystal structure of the yeast eIF4A-eIF4G complex: an RNA-helicase controlled by protein-protein interactions. Proc. Natl. Acad. Sci. U S A *105*, 9564–9569.

Shao, C., Yang, B., Wu, T., Huang, J., Tang, P., Zhou, Y., Zhou, J., Qiu, J., Jiang, L., Li, H., et al. (2014). Mechanisms for U2AF to define 3' splice sites and regulate alternative splicing in the

human genome. Nat. Struct. Mol. Biol. *21*, 997–1005.

Shi, J., Luo, L., Eash, J., Ibebunjo, C., and Glass, D.J. (2011). The SCF-Fbxo40 complex induces IRS1 ubiquitination in skeletal muscle, limiting IGF1 signaling. Dev. Cell *21*, 835–847.

Singh, R.K., Xia, Z., Bland, C.S., Kalsotra, A., Scavuzzo, M.A., Curk, T., Ule, J., Li, W., and Cooper, T.A. (2014). Rbfox2-coordinated alternative splicing of Mef2d and Rock2 controls myoblast fusion during myogenesis. Mol. Cell *55*, 592–603.

Sinha, R., Allemand, E., Zhang, Z., Karni, R., Myers, M.P., and Krainer, A.R. (2010). Arginine methylation controls the subcellular localization and functions of the oncoprotein splicing factor SF2/ASF. Mol. Cell. Biol. *30*, 2762–2774.

Skarnes, W.C., Rosen, B., West, A.P., Koutsourakis, M., Bushell, W., Iyer, V., Mujica, A.O., Thomas, M., Harrow, J., Cox, T., et al. (2011). A conditional knockout resource for the genome-wide study of mouse gene function. Nature *474*, 337–342.

Tian, B., and Manley, J.L. (2013). Alternative cleavage and polyadenylation: the long and short of it. Trends Biochem. Sci. *38*, 312–320.

Wang, H., Huang, Z.Q., Xia, L., Feng, Q., Erdjument-Bromage, H., Strahl, B.D., Briggs, S.D., Allis, C.D., Wong, J., Tempst, P., et al. (2001). Methylation of histone H4 at arginine 3 facilitating transcriptional activation by nuclear hormone receptor. Science *293*, 853–857.

Wei, C., Qiu, J., Zhou, Y., Xue, Y., Hu, J., Ouyang, K., Banerjee, I., Zhang, C., Chen, B., Li, H., et al. (2015). Repression of the central splicing regulator RBFox2 is functionally linked to pressure overload-induced heart failure. Cell Rep. *10*, 1521–1533.

Wells, Q.S., Becker, J.R., Su, Y.R., Mosley, J.D., Weeke, P., D'Aoust, L., Ausborn, N.L., Ramirez, A.H., Pfotenhauer, J.P., Naftilan, A.J., et al. (2013). Whole exome sequencing identifies a causal RBM20 mutation in a large pedigree with familial dilated cardiomyopathy. Circ. Cardiovasc. Genet. *6*, 317–326.

Xu, X., Yang, D., Ding, J.H., Wang, W., Chu, P.H., Dalton, N.D., Wang, H.Y., Bermingham, J.R., Jr., Ye, Z., Liu, F., et al. (2005). ASF/SF2-regulated CaMKIIdelta alternative splicing temporally reprograms excitation-contraction coupling in cardiac muscle. Cell *120*, 59–72.

Yamagata, K., Daitoku, H., Takahashi, Y., Namiki, K., Hisatake, K., Kako, K., Mukai, H., Kasuya, Y., and Fukamizu, A. (2008). Arginine methylation of FOXO transcription factors inhibits their phosphorylation by Akt. Mol. Cell *32*, 221–231.

Yang, Y., and Bedford, M.T. (2013). Protein arginine methyltransferases and cancer. Nat. Rev. Cancer *13*, 37–50.

Yang, Y., Hadjikyriacou, A., Xia, Z., Gayatri, S., Kim, D., Zurita-Lopez, C., Kelly, R., Guo, A., Li, W., Clarke, S.G., et al. (2015). PRMT9 is a type II methyltransferase that methylates the splicing factor SAP145. Nat. Commun. *6*, 6428.

Ye, J., Beetz, N., O'Keeffe, S., Tapia, J.C., Macpherson, L., Chen, W.V., Bassel-Duby, R.,

Olson, E.N., and Maniatis, T. (2015). hnRNP U protein is required for normal pre-mRNA splicing and postnatal heart development and function. Proc. Natl. Acad. Sci. U S A *112*, E3020–E3029.

Ye, J., Zhang, Y., Xu, J., Zhang, Q., and Zhu, D. (2007). FBXO40, a gene encoding a novel muscle-specific F-box protein, is upregulated in denervation-related muscle atrophy. Gene *404*, 53–60.

Zhang, L., Tran, N.T., Su, H., Wang, R., Lu, Y., Tang, H., Aoyagi, S., Guo, A., Khodadadi-Jamayran, A., Zhou, D., et al. (2015). Cross-talk between PRMT1-mediated methylation and ubiquitylation on RBM15 controls RNA splicing. Elife *4*, e07938.

Zurita-Lopez, C.I., Sandberg, T., Kelly, R., and Clarke, S.G. (2012). Human protein arginine methyltransferase 7 (PRMT7) is a type III enzyme forming omega-NG-monomethylated arginine residues. J. Biol. Chem. *287*, 7859–7870.

Supplemental Information

PRMT1 Deficiency in Mouse Juvenile Heart

Induces Dilated Cardiomyopathy and Reveals

Cryptic Alternative Splicing Products

Kazuya Murata, Weizhe Lu, Misuzu Hashimoto, Natsumi Ono, Masafumi Muratani, Kana Nishikata, Jun-Dal Kim, Shizufumi Ebihara, Junji Ishida, and Akiyoshi Fukamizu

Supplemental Figures and Tables
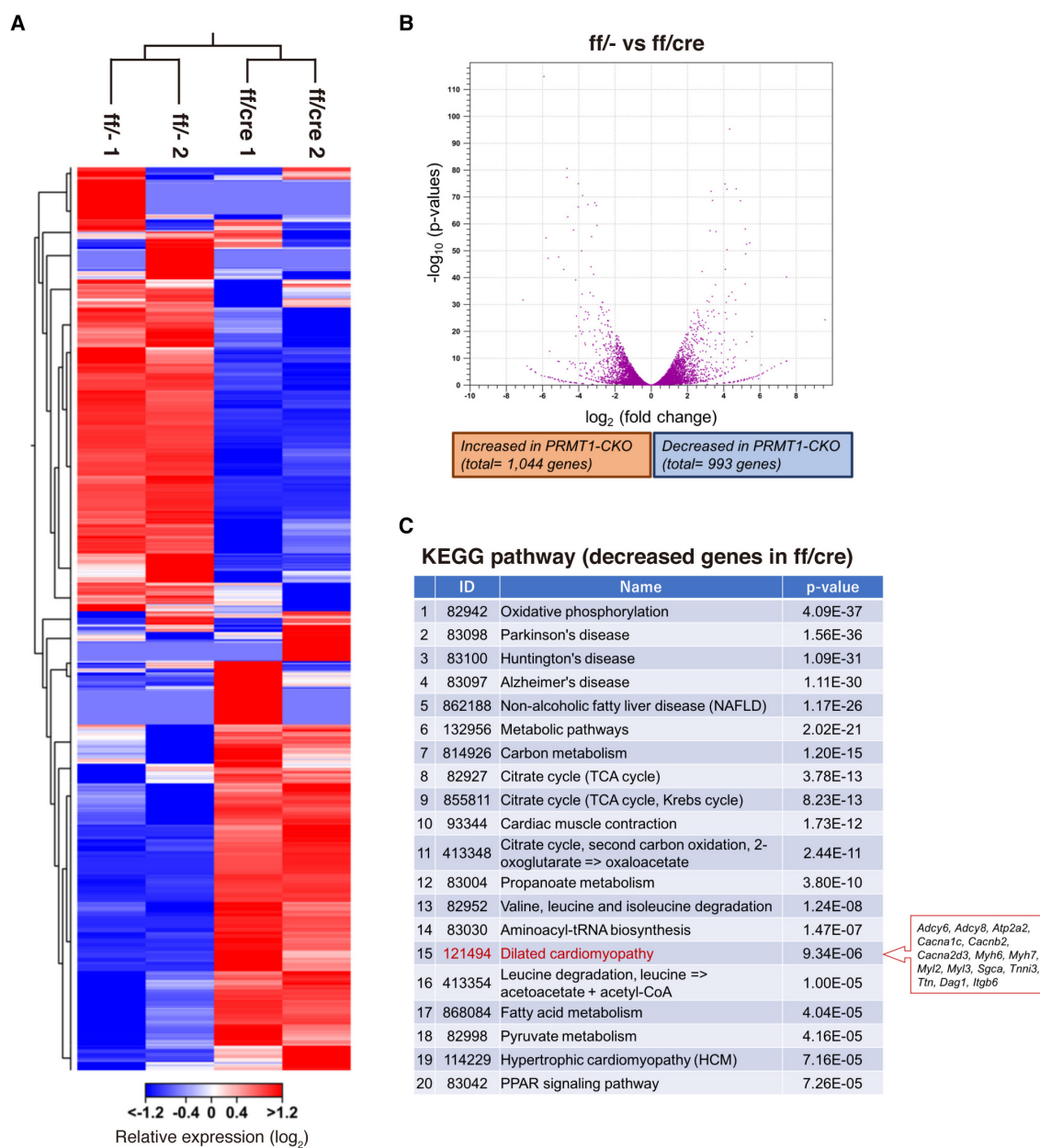
Figure S1 (related to Figure 3). Gene expression profile of RNA-Seq data

(A and B) A hierarchical clustering and a volcano plot based on the 2,037 differentially expressed genes between control and PRMT1-cKO group (adjusted FDR *P* value < 0.05). (C) Functional enrichment analysis of 993 downregulated genes in PRMT1-cKO mice. The top 20 enriched pathways are shown in the table. A list of matched genes with DCM-related gene sets in the box insert. See also Table S1.

GO biological process

FDR-adjusted p-value

1.E-01	1.E-04	1.E-07

Striated muscle cell development

Muscle cell development

Muscle system process

Muscle structure development

Muscle cell differentiation

Striated muscle cell differentiation

Myofibril assembly

Striated muscle contraction

Actin cytoskeleton organization

Cardiac muscle cell development
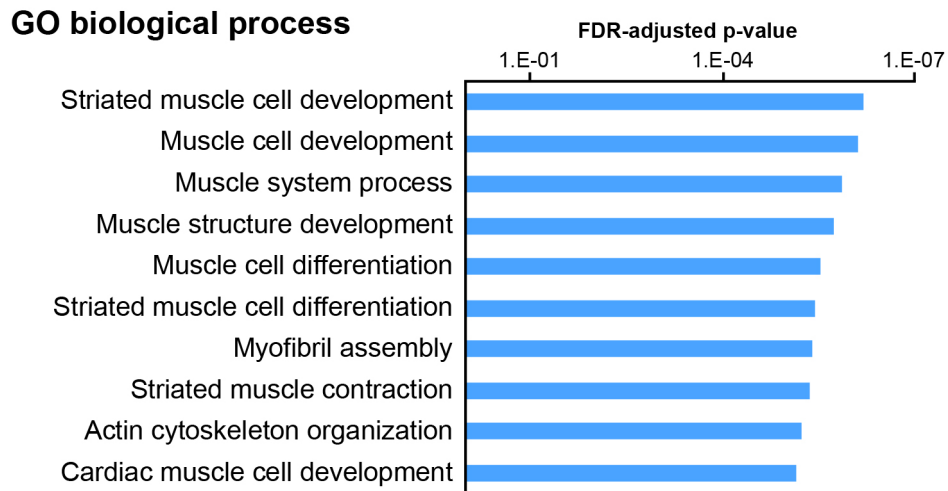
Figure S2 (related to Figure 4). Gene ontology (GO) analysis of alternatively expressed isoforms between control and PRMT1-cKO mice

GO analysis of 74 genes was performed using the PANTHER web tool (Mi et al., 2013). The top 10 enriched GO terms are shown in the graph.
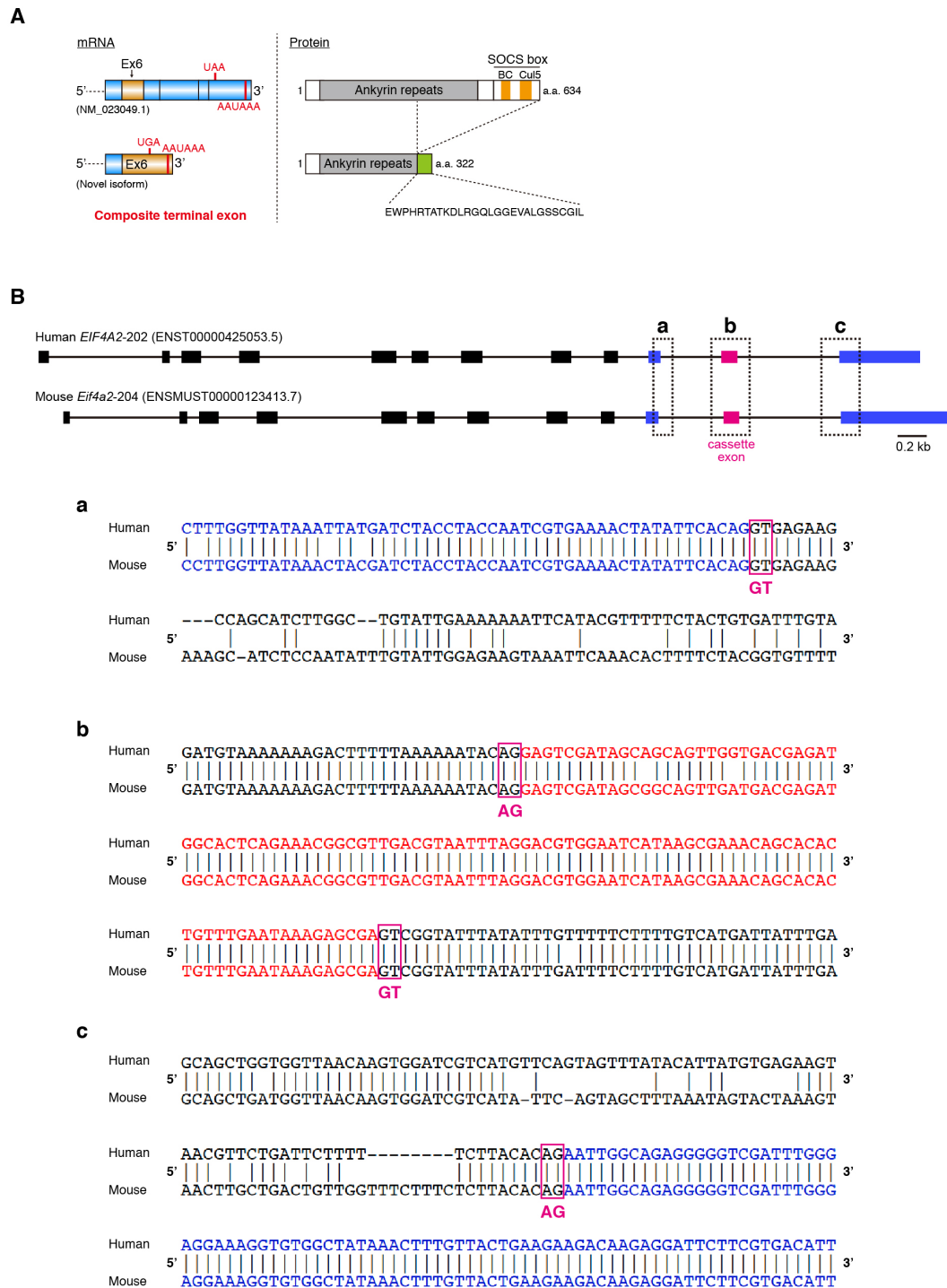
Figure S3 (related to Figure 4). Schematic diagrams of *Asb2* mRNA/protein and *Eif4a2* gene

(A) 3' side of *Asb2* mRNA and domain structure of ASB2 protein. The extended exon 6 contains a stop codon and a putative poly(A) signal. (B) Structures of human and mouse *Eif4a2* transcripts. (a-c) DNA sequences surrounding splice donor and acceptor sites.

Alternatively spliced genes	Animal models	Reference	
Tmed2, Snap23	CELF1-overexpressing mice	*Nat. Commun.* 2014	doi: 10.1038/ncomms4603.
Mef2a	SRSF10-KO mice	*Cell Rep.* 2015	doi: 10.1016/j.celrep.2015.10.038.
	RBFOX2-KO mice	*Cell Rep.* 2015	doi: 10.1016/j.celrep.2015.02.013.
Ktn1	CELF1-KO mice	*Sci. Rep.* 2016	doi: 10.1038/srep35550.
	rbfox1-KD zebrafish	*J. Cell Sci.* 2015	doi: 10.1242/jcs.166850.
Lmo7	RBM20-KO rats	*J. Clin. Invest.* 2014	doi: 10.1172/JCI74523.
Srobs1	MBNL1-KO mice	*Sci. Rep.* 2015	doi: 10.1038/srep09042.
	RBFOX2-KO mice	*Cell Rep.* 2015	doi: 10.1016/j.celrep.2015.02.013.
	RBM20-KO rats	*Nat. Med.* 2012	doi: 10.1038/nm.2693.
Ttn	RBM20-KO rats	*Nat. Med.* 2012	doi: 10.1038/nm.2693.
	hnRNPU-KO mice	*Proc. Natl. Acad. Sci. U. S. A.* 2015	doi: 10.1073/pnas.1508461112.

Table S2 (related to Figure 3). Summary of known cardiac alternative splicing events that were investigated as illustrated in Figure 3.

Feature ID	P-value	Relative RPKM	Relative RPKM	WT Means	Relative RPKM	Relative RPKM	KO Means	Ratio
Sptan1_11	7.86E-03	3.41E-04	1.84E-04	2.16E-03	0.28	0.21	4.63	0.00107
Acp5_1	5.00E-04	0.04	0	4.41E-03	1	1	7.02	0.02000
Ppfibp1_3	4.95E-04	0.03	3.17E-03	0.08	0.57	0.83	6.87	0.02369
Ndrg4_6	9.88E-04	6.17E-03	0	0.07	0.1	0.13	6.29	0.02683
Fbxo40_3	2.81E-04	0.02	0.02	0.28	0.21	0.42	8.87	0.06349
Fam198b_1	0.04	0.09	0	0.14	0.53	0.67	4.8	0.07500
Smdt1_2	6.43E-03	0	0.06	0.47	0.18	0.56	6.37	0.08108
Nrap_5	1.52E-03	0.05	0.09	0.89	0.71	1	10.33	0.08187
Tnnt2_4	0.04	1.18E-03	0	0.3	5.25E-03	7.28E-03	4.29	0.09417
1500017E21Rik_4	0.02	0.06	0.12	0.1	0.7	1	4.03	0.10588
Tpm1_12	5.94E-13	0.01	9.71E-03	14.67	0.1	0.07	108.86	0.11594
Gsn_4	4.53E-03	2.51E-03	9.42E-03	0.92	0.03	0.06	8.97	0.13256
Atpif1_1	6.61E-05	0	0.18	3.1	0.34	1	26.8	0.13433
Nptn_4	7.57E-03	0.16	0.01	0.87	0.9	0.29	7.26	0.14286
Synpo2l_3	9.91E-04	0.16	0.16	0.36	1	1	8.01	0.16000
Ttn_14	1.36E-03	0.13	0.15	14.01	0.76	0.95	40.95	0.16374
Clu_3	5.51E-07	0.01	4.87E-03	0.56	0.03	0.06	16.15	0.16522
Cxcl12_1	0.05	0.16	0.2	1.62	1	1	7.54	0.18000
Vmp1_2	0.04	0.08	0.12	0.34	0.59	0.5	4.31	0.18349
Fhl1_2	1.34E-10	0.19	0.18	1.45	1	1	29.04	0.18500
H19_5	0.02	0.05	5.56E-03	0.06	0.15	0.14	4	0.19159
Pkm_1	3.25E-05	0.04	0.05	3.24	0.28	0.18	21.89	0.19565
Pdlim5_5	7.81E-03	0.05	0.04	3.88	0.23	0.22	15.37	0.20000
Tnnt2_1	0.04	3.55E-03	5.55E-04	1.07	9.82E-03	0.01	6.96	0.20711
Sptan1_9	0.01	0.12	0.04	0.68	0.47	0.26	6.74	0.21918
Casq2_1	0.01	4.13E-03	0.05	2.16	0.15	0.09	10.31	0.22554
Popdc2_1	0.02	0.08	0.06	2.62	0.21	0.29	11.48	0.28000
Sorbs2_7	2.27E-04	0.08	0.09	0.68	0.3	0.28	11.05	0.29310
Rhod_2	0.02	0.29	0.37	0.18	1	1	5.41	0.33000
Lamp2_3	2.82E-04	0.33	0.34	5.13	1	1	22.74	0.33500
Postn_5	6.56E-09	0.09	0.31	0.75	0.64	0.54	22.36	0.33898
Ldb3_5	2.77E-03	0.31	0.37	18.39	1	1	11.19	0.34000
Strn_3	0.04	0.1	0.32	0.34	0.6	0.62	4.62	0.34426
Fez2_1	0.02	0.33	0.36	2.42	1	1	10.51	0.34500
Aldoa_9	4.99E-11	0.16	0.24	44.49	0.52	0.55	136.5	0.37383
Ptpn11_2	1.36E-03	0.36	0.29	2.59	0.83	0.76	14.73	0.40881
Myl4_7	9.86E-03	0.17	0	8.84	0.2	0.21	32.27	0.41463
Mybpc3_1	0.02	7.13E-03	6.19E-03	1.27	0.02	0.01	7.54	0.44400
Ctsd_4	2.21E-03	0.05	0.04	2.83	0.14	0.05	17.84	0.47368
P4hb_1	0.02	0.05	0.08	1.17	0.18	0.09	7.36	0.48148
Tnnt2_7	8.29E-03	0.11	0.05	43.03	0.17	0.16	114.35	0.48485
Rtn4_6	3.46E-03	0	0.06	0.15	0.07	0.05	7.05	0.50000
Tfpi_10	0.01	0.37	0.33	1.66	0.76	0.64	8.93	0.50000
Ccdc141_9	7.63E-03	1	0.95	6.42	0.63	0.34	1.93	2.01031
Smtn_5	0.03	1	1	2.78	0.48	0.51	0.39	2.02020
Coro6_6	7.86E-03	0.33	0.36	3.59	0	0.34	0.32	2.02941
Hint2_1	0.04	0.44	0.35	3.46	0.17	0.2	0.87	2.13514
Osgepl1_1	0.04	1	0.92	3.38	0.68	0.21	0.76	2.15730
Kcnj3_1	0.02	1	1	2.9	0.54	0.34	0.28	2.27273
Ivns1abp_2	2.80E-03	0.21	0.19	18.34	0.06	0.11	10.89	2.35294
Adck3_11	0.02	0.07	0.12	3.15	0	0.08	0.22	2.37500
Mrpl51_2	0.04	0.2	0.26	3.38	0.13	0.06	0.77	2.42105
Echs1_5	0.03	0.05	0.05	2.49	0.02	0.02	0.37	2.50000
Oxct1_3	8.95E-06	0.12	0.16	12.2	0.09	0.02	2.28	2.54545
Bsg_1	8.32E-06	0.31	0.35	43.58	0.04	0.21	12.22	2.64000
Ctgf_2	0.01	0.19	0.18	2.09	0.07	0.07	10.39	2.64286
Myl2_8	7.47E-03	2.38E-03	1.59E-03	5.89	2.67E-04	1.18E-03	1.12	2.74361
Obscn_6	1.52E-03	1	1	7.84	0.53	0.18	2.18	2.81690
Myl2_12	1.25E-04	3.32E-03	2.78E-03	9.03	5.44E-04	1.58E-03	1.66	2.87194
Cdh13_3	0.04	0.27	0.38	3.72	0.16	0.06	0.78	2.95455
Nudt7_5	6.41E-03	0.34	0.83	4.94	0.35	0.03	0.52	3.07895
Ndufs1_2	1.24E-04	0.19	0.18	8.86	0.06	0.06	1.22	3.08333
Ttn_19	3.71E-05	0.1	0.1	9.84	0.03	0.03	1.41	3.33333
Ttn_6	3.45E-03	0.05	0.05	5.17	0.01	0.02	0.85	3.33333
Lmo7_16	2.65E-03	0.57	0.68	8.32	0.19	0.18	2.63	3.37838
Mtch2_6	0.01	0.33	0.46	5.17	0.17	0.06	1.21	3.43478
Chpt1_5	4.45E-07	0.92	1	14.35	0.35	0.19	2.25	3.55556
Asb2_2	1.51E-05	1	1	14.6	0.35	0.2	3.89	3.63636
Eif4a2_17	5.02E-05	0.64	0.8	19.4	0.23	0.16	8.44	3.69231
D4Wsu53e_3	0.02	0.29	0.19	3.83	0.07	0.05	0.76	4.00000
Ech1_5	7.92E-09	0.06	0.07	12.41	8.63E-03	0.02	0.52	4.54069
Narf_2	0.04	0.39	0.39	3.57	0.05	0.12	0.52	4.58824
Smdt1_3	5.01E-04	0.48	0.52	8.9	0.17	0	1.81	5.88235
Slc25a39_14	0.04	0.79	0.78	3.32	0.06	0.18	0.97	6.54167
Ttll1_4	7.86E-03	1	1	3.74	0.29	0	0.2	6.89655
Sgca_2	3.45E-03	0.73	1	5.41	0.07	0.17	0.73	7.20833
Gpcpd1_13	0.03	0.09	0.14	2.65	0.02	0.01	0.2	7.66667
Obscn_5	1.97E-03	0.5	0.59	4.26	0.05	0.06	0.36	9.90909
Acot7_6	0.02	1	0.43	3.12	0.08	0.04	0.27	11.91667
Mff_10	3.94E-03	0.52	1	4.19	0.05	3.25E-03	0.18	28.54460
Ift81_2	3.93E-03	1	1	3.88	0	0.03	0.02	66.66667
Ndufv1_1	0.03	0.02	0.06	2.67	0	4.97E-04	9.19E-03	160.96579

Table S3 (related to Figure 4). Candidate genes exhibiting aberrant alternative splicing in PRMT1-cKO mice.

Transparent Methods

Animal experiments

PRMT1^{KI} mice that carry *Prmt1$^{tm1a(EUCOMM)Wtsi}$* allele and *Prmt1$^{flox/flox}$* mice were obtained and generated as previously described (Hashimoto et al., 2016). To create PRMT1-cKO mice, *Prmt1$^{flox/flox}$* mice were mated with αMHC-cre transgenic mice (strain name: B6.FVB-Tg(Myh6-cre)2182Mds/J, stock number: 011038, The Jackson Laboratory). C57BL/6J mice were purchased from CLEA Japan for isolation of primary cardiomyocytes and non-myocytes. Genotype of PRMT1-cKO mice was determined by PCR and agarose gel electrophoresis. Briefly, a small piece of tail was removed from 10-14-day-old mice, and direct PCR was performed using HelixAmp Direct PCR 3G (NanoHelix #DPR200) in accordance with the manufacturer's instructions. The primer sequences were as follows: *Prmt1* (5'-GTGCTTGCCATACAAGAGATCC-3' and 5'-GTGAAACATGGAGTTGCGGTAT-3'); αMHC-cre transgene (5'-ATGACAGACAGATCCCTCCTATCTCC-3' and 5'-CTCATCACTCGTTGCATCATCGAC-3'). To assess cardiac contractile function, echocardiography was performed as described previously (Murata et al., 2013). Male mice were used for all experiments except X-gal staining.

All animal experiments were performed in a humane manner and approved by the Institutional Animal Experiment Committee of the University of Tsukuba. Experiments were conducted in accordance with the Regulations for Animal Experiments of the University of Tsukuba and the Fundamental Guidelines for Proper Conduct of Animal Experiments and Related Activities in Academic Research Institutions under the jurisdiction of the Ministry of Education, Culture, Sports, Science and Technology of Japan.

Histological analysis

Hearts were embedded in paraffin and sectioned as previously described (Murata et al., 2013). Deparaffinized cardiac sections (5 and 3 μm thick) were stained with hematoxylin-eosin (HE) and Masson's trichrome reagents. Images were obtained using a BX53 microscope and DP21 digital camera (Olympus).

For immunohistochemistry, deparaffinized cardiac sections (5 μm thick) were placed in 10 mM sodium citrate buffer (pH 6.0), boiled 20 seconds in a microwave oven, and cooled at room temperature for 20 minutes. To inactivate endogenous peroxidase, sections were incubated with 3% H_2O_2 for 30 minutes. After incubation with TSA blocking reagent (Perkin Elmer, #FP1020)

for 30 minutes, sections were incubated with anti-PRMT1 antibody (1:200, rabbit-monoclonal, abcam, #ab92299) at room temperature for 60 minutes. Sections were then reacted with biotinylated anti-rabbit antibody (1:500, Vector, #BA1000) for 30 minutes at room temperature. Secondary antibodies were detected using the tyramide signal amplification (TSA) Plus Fluorescein System (Perkin Elmer, #NEL756001KT). For double-staining, sections were incubated with anti-cardiac troponin I antibody (1:50, rabbit-polyclonal, abcam, #ab47003) for 60 minutes at room temperature. Primary antibodies were visualized using Alexa Fluor 568 conjugated secondary antibody (Thermo Fisher Scientific, A11011). CF640R conjugated wheat germ agglutinin (WGA, Biotium, #29026) and Hoechst 33258 were used to stain cellular membranes and nuclei. Fluorescent images were obtained using a FluoView FV10i confocal laser-scanning microscope (Olympus).

X-gal staining

For X-gal staining, 8-week-old mice were perfused with 4% paraformaldehyde (PFA), then the heart tissues were dissected, following immersion fixation in 4% PFA for 15 minutes. The hearts from E19 embryos were harvested and fixed with 4% PFA for 15 minutes. Tissues were then cryoprotected, embedded in O.C.T. compound, and cryostat sectioned. Sections were stained in 1xPBS containing 1 mg/ml X-gal, 5 mM $K_4Fe(CN)_6/3H_2O$, 5 mM $K_3Fe(CN)_6$, 2 mM $MgCl_2$, 0.05% sodium deoxycholate, and 0.02% NP-40 at 37°C overnight. Slides were then counter-stained with eosin. Data images were obtained using a BX53 microscope and DP21 digital camera (Olympus).

Western blotting

Immunoblot analysis was performed as previously described (Murata et al., 2016). The primary antibodies were as follows: anti-PRMT1 (1:500-1:1000, Millipore, #07-404), anti-cardiac troponin I (1:250, Santa Cruz Biotechnology, #sc-31655), anti-vimentin (1:1000, Cell Signaling Technology, #5741), anti-GAPDH (1:2000-1:10000, American Research Products, #05-50118).

Cardiomyocyte isolation

Ventricles harvested from neonatal mice were minced and enzymatically digested in HBSS (with Mg^{2+}) containing 0.45 mg/ml collagenase type II (Worthington, #CLS2) and 0.11 mg/ml pancreatin (GIBCO, #002-0036DG) at 37°C with gentle shaking and intermittent pipetting. Cell suspension was collected and filtered through a cell strainer (40 μm nylon mesh). The cells

were collected by centrifugation, resuspended in cardiomyocyte (CM) growth medium (DMEM/M199 (4:1) with 10% horse serum (HYCLONE, #SH30074.03), 5% fetal bovine serum (FBS), 1.6 mM L-glutamine (Life Technologies, #25030-081), 80 µM non-essential amino acid (GIBCO, #11140-050), and penicillin-streptomycin (PS)), and plated on non-coated plastic dishes. After 2.5 hours incubation with 5% CO_2 at 37ºC, the non-adhesive cells (cardiomyocytes) were collected, resuspended in CM growth medium containing 25 µM cytosine β-D-arabinofuranoside (Ara-C, SIGMA, #C1768), and plated on gelatin-coated dishes. The remaining adhesive cells (non-myocytes) were grown in DMEM supplemented with 10% FBS and PS.

RNA experiments

Cardiac RNA was extracted using mirVana miRNA Isolation Kit (Thermo Fisher Scientific, #AM1560) in accordance with the manufacturer's instructions. Large RNA fraction containing mRNA was used for gene expression assay. Reverse transcription and quantitative real-time-PCR was performed as described previously (Murata et al., 2013, Murata et al., 2016).

To validate alternative splicing events, RT-PCR was performed using AmpliTaq Gold DNA Polymerase (Thermo Fisher Scientific, #4398881) and PrimeSTAR Max DNA Polymerase (for detecting *Fbxo40* isoforms, TAKARA, #R045A). PCR products were separated by 8.5% acrylamyde gel electrophoresis and stained with ethidium bromide. Images were acquired using an LAS-3000 imaging system (GE healthcare) and analyzed by ImageJ software (National Institutes of Health). Percent spliced in (PSI) value was calculated from the band intensity, as previously described (Giudice et al., 2014). The primers for RT-PCR were as follows:

Tmed2-forward (5'-GTACACATTTGCAGCCCACA-3')

Tmed2-reverse (5'-CTCCTGTTCGTGCTTTACGG-3')

Snap23-forward (5'-GTGTTGTGGCCTCTGCATCT-3')

Snap23-reverse (5'-TGGCTGCTCCTGTAGTTTGCT-3')

Mef2a-forward (5'-AACTCAAGGGCCTCTCCAAA-3')

Mef2a-reverse (5'-CACTACAGGCGTGGCAAGAG-3')

Ktn1-forward (5'-GATCCATGAGAAAGATGGACAGA-3')

Ktn1-reverse (5'-GCAGCTCCTGGACTTGAGAA-3')

Lmo7-forward (5'-TGAGCCAAAGTCAGCTCTCC-3')

Lmo7-reverse (5'-ACTTGCTCCCATTCTCACCA-3')

Sorbs1-forward (5'-AGACCTTCGTCTGCCTACCC-3')

Sorbs1-reverse (5'-GCATCCTTTGCCCTTCTCTC-3')

Ttn (exon 47-48)-forward (5'-CCAGGCCGAGTTGACCATCA-3')

Ttn (exon 47-48)-reverse (5'-GCAATGGAGGCGTGCTGATT-3')

Ttn (exon 48-50)-forward (5'-CAGCACGCCTCCATTGCAAG-3')

Ttn (exon 48-50)-reverse (5'-CAGGGATGGTCAAGACGGCA-3')

Ttn (exon 132-134)-forward (5'-TCGGGAGGAGGAGTATGAGG-3')

Ttn (exon 132-134)-reverse (5'-GGGTGGCAGAGGTTTGAGTT-3')

Ttn (exon 147-150)-forward (5'-GCTCCCACTCCTGTCCCTAA-3')

Ttn (exon 147-150)-reverse (5'-CACCCTGATGAACTCCTCCAC-3')

Asb2 (exon 6-7)-forward (5'-CAGCATCACCCCTTTGTTTG-3')

Asb2 (exon 6-7)-reverse (5'-TCATTCTTGCTGGCCTCGT-3')

Asb2 (extended ex6)-forward (5'-CAGCATCACCCCTTTGTTTG-3')

Asb2 (extended ex6)-reverse (5'-CCTGGCCTAAGAGTCCTCCA-3')

Fbxo40-forward (5'-AGAAGCCAGAAGCAGGGAAG-3')

Fbxo40-reverse (5'-GCTCCACGATGTTGAAAGGA-3')

Nrap-forward (5'-TGTTGCTTCTCCCTGTCTCC-3')

Nrap-reverse (5'-GGCTGCCACAGACTTCTTCA-3')

Eif4a2-forward (5'-TGACGTGCAACAAGTGTCCT-3')

Eif4a2-reverse (5'-CCACACCTTTCCTCCCAAA-3')

RNA sequencing

For the preparation of cDNA library, total RNA was extracted from the heart of 6 weeks-old mice (n = 2) using ISOGEN II (Nippon Gene, #311-07361). Ribosomal RNA (rRNA) was removed using RiboMinus Eukaryote Kit (Thermo Fisher Scientific, #A1083708). Depletion of rRNA was confirmed using the Agilent 2100 Bioanalyzer (Agilent Technologies). cDNA libraries were then prepared using SOLiD total RNA-Seq kit (Thermo Fisher Scientific, #4445374) in accordance with the manufacturer's instructions. Briefly, rRNA-depleted RNA was fragmented by RNase III, and subsequently incubated with T4 polynucleotide kinase. After purification of fragmented RNA, the size of fragmented RNA was determined using the Agilent 2100 Bioanalyzer. Fragmented RNA was ligated to SOLiD adaptor, and reverse transcribed by ArrayScript reverse transcriptase (Thermo Fisher Scientific). The cDNA was purified using Agencourt AMPure XP (Beckman Coulter), and amplified by 15 cycles of PCR using SOLiD barcoded 3' primers. Amplified cDNA was purified and size-selected using Agencourt AMPure

XP. The quality of the cDNA library was checked by the Agilent 2100 Bioanalyzer, and quantified by TaqMan qPCR. RNA sequencing was carried out using the 5500xl SOLiD system (Thermo Fisher Scientific) in the single-end sequencing mode (75 bp reads) in accordance with the manufacturer's instructions.

The data were imported into CLC Genomics Workbench software (v9.5.3, Qiagen), and mapped to the mouse genome (GRCm38) using RNA-sequencing analysis tool. Transcript expression was analyzed against 83,260 transcript models downloaded from the CLC website. Quantification value for each transcript was obtained in RPKM (reads per kilobase per million reads), and used for empirical analysis of DGE in CLC Genomics Workbench. RNA isoforms were filtered based on significant expression changes ($p < 0.05$) between control and PRMT1-cKO mice samples. Relative expression of isoforms between two groups was then compared by calculating isoform ratio in the following manner:

Relative RPKM = transcript-specific RPKM / total RPKM from transcript isoforms

(means of N=2, respectively)

Isoform ratio = Relative RPKM in WT / Relative RPKM in cKO

By filtering for changes at least 2.0-fold, 82 transcripts (74 genes) were selected as candidate splicing regulation events. To visually confirm these splicing events, BAM files were exported from CLC Genomics Workbench, sorted, imported to into the Integrative Genomics Viewer (IGV), and Sashimi plot images were created.

Data and software availability

The accession number for the data reported in this study is GEO: GSE112938.

Gene ontology (GO) analysis

GO overrepresentation test was performed using the PANTHER web tool (http://pantherdb.org). The gene list (74 genes) was uploaded and analyzed by statistical overrepresentation test (Fisher's Exact with FDR multiple test correction; Annotation Version and Release Date: GO Ontology database Released 2018-07-03).

Cell culture

C2C12 mouse myoblasts were grown in DMEM supplemented with 10% FBS and PS (growth medium). Cell differentiation was induced by switching from growth medium to DMEM containing 2% horse serum and PS. At three days after induction of differentiation, cells were

collected and used for mRNA experiment.

Transfection and immunoprecipitation assay

To investigate the function of eIF4A2 isoforms, mouse eIF4A2 isoforms were amplified by PCR from heart cDNA and inserted into pHA-C1 vector.

The primers for cDNA cloning were as follows:

XhoI-eIF4A2-forward (5'-CCGCTCGAGCTATGTCTGGTGGCTCCGCGGA-3')

eIF4A2-wt-BamHI-reverse (5'-CGCGGATCCTTAAATTAGGTCAGCCACAT-3')

eIF4A2-tr-BamHI-reverse (5'-CGCGGATCCCTATCGACTCCTGTGAATAT-3')

For detecting ubiquitination, plasmids were transfected into C2C12 cells using Lipofectamine LTX (Thermo Fisher Scientific, #5338100) in accordance with the manufacturer's instructions. After 16 hours incubation, cells were treated with MG132 (10 μM final concentration, Enzo Life Sciences, #BML-PI102-0005) for 8 hours. Cells were lysed in ice-cold TNE buffer containing 0.1% Triton X-100. After centrifugation, the supernatants were incubated overnight with anti-HA antibody (Roche, #11867423001) at 4ºC. To collect the immunocomplex, SureBeads Protein G Magnetic Beads (Bio-Rad, #1614023) were added to samples. After incubation for 1 hour at 4ºC, the beads were washed three times with lysis buffer, 2xSDS sample buffer was added, and incubated for 5 minutes at 99°C. Immunoblot was performed using following primary antibodies: anti-HA (1:2000, mouse-monoclonal, Wako, #014-21881), anti-ubiquitin (1:500, mouse-monoclonal, Santa Cruz Biotechnology, #sc-8017), anti-β-actin (1:2000, rabbit-polyclonal, Medical & Biological Laboratory, #PM053).

Statistical analysis

Statistical analysis was performed using GraphPad Prism 5 (GraphPad Prism Software). The data were analyzed using Student's *t*-test and Mann Whitney test, and two-way ANOVA followed by Bonferroni multiple comparison test. Significant differences were defined as $p < 0.05$.

Supplemental references

Mi, H., Muruganujan, A., Casagrande, J.T., and Thomas, P.D. (2013). Large-scale gene function analysis with the PANTHER classification system. Nat. Protoc. *8*, 1551-1566.

Murata, K., Ishida, J., Ishimaru, T., Mizukami, H., Hamada, J., Saito, C., and Fukamizu, A. (2016). Lactation Is a Risk Factor of Postpartum Heart Failure in Mice with Cardiomyocyte-specific Apelin Receptor (APJ) Overexpression. J. Biol. Chem. *291*, 11241-11251.

Murata, K., Saito, C., Ishida, J., Hamada, J., Sugiyama, F., Yagami, K., and Fukamizu, A. (2013). Effect of lactation on postpartum cardiac function of pregnancy-associated hypertensive mice. Endocrinology *154*, 597-602.